Lecture 3:
The circulation of the stratosphere and mesosphere

(i) The observed mean state, and the deduced meridional circulation
(ii) Stratospheric Rossby waves
(iii) Rossby waves and the stratospheric circulation
(iv) Gravity waves and the mesospheric circulation
(v) Variability of the stratospheric circulation: wintertime vacillations and polar warmings
(vi) Variability of the stratospheric circulation: the tropical quasi-biennial oscillation

FDEPS 2010
Alan Plumb, MIT
Nov 2010

(i) The observed mean state, and the deduced meridional circulation

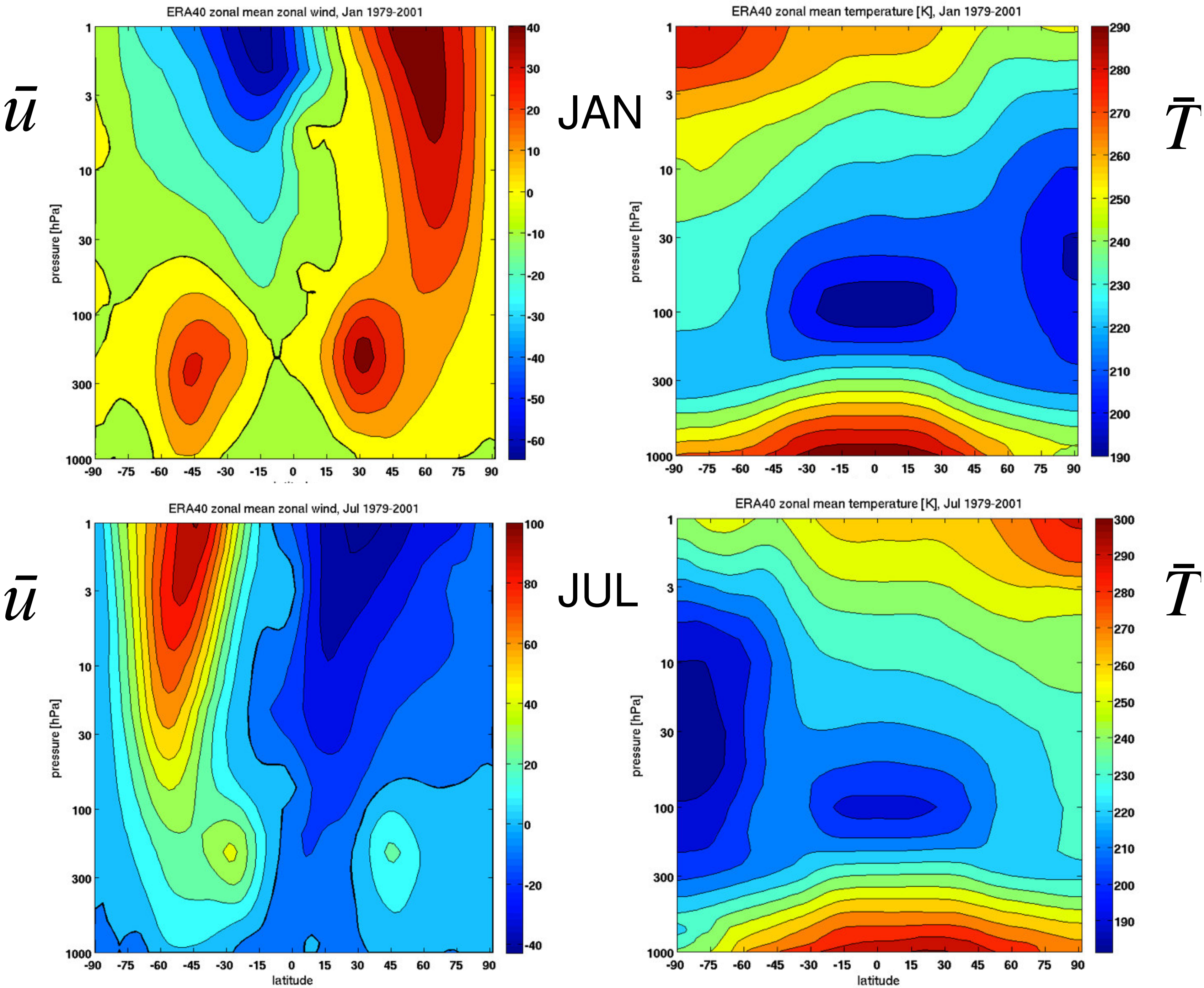
ERA40 zonal mean zonal wind, Jan 1979-2001
ERA40 zonal mean temperature [K], Jan 1979-2001
ERA40 zonal mean zonal wind, Jul 1979-2001
ERA40 zonal mean temperature [K], Jul 1979-2001
$\bar{u}$
$\bar{T}$
JAN
JUL
pressure [hPa]
latitude

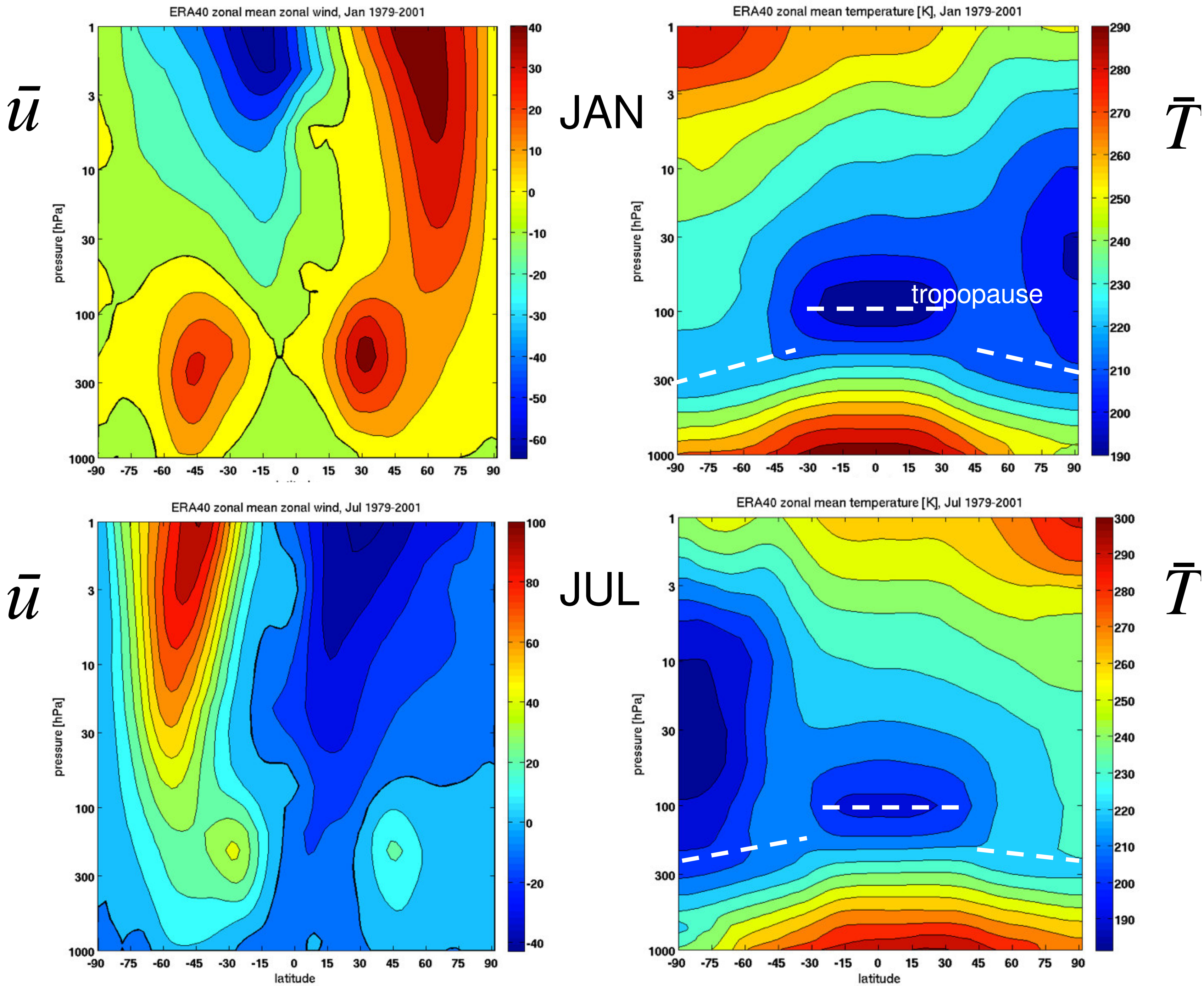

$\bar{u}$
JAN
$\bar{T}$
ERA40 zonal mean zonal wind, Jan 1979-2001
ERA40 zonal mean temperature [K], Jan 1979-2001
tropopause
$\bar{u}$
JUL
$\bar{T}$
ERA40 zonal mean zonal wind, Jul 1979-2001
ERA40 zonal mean temperature [K], Jul 1979-2001
pressure [hPa]
latitude

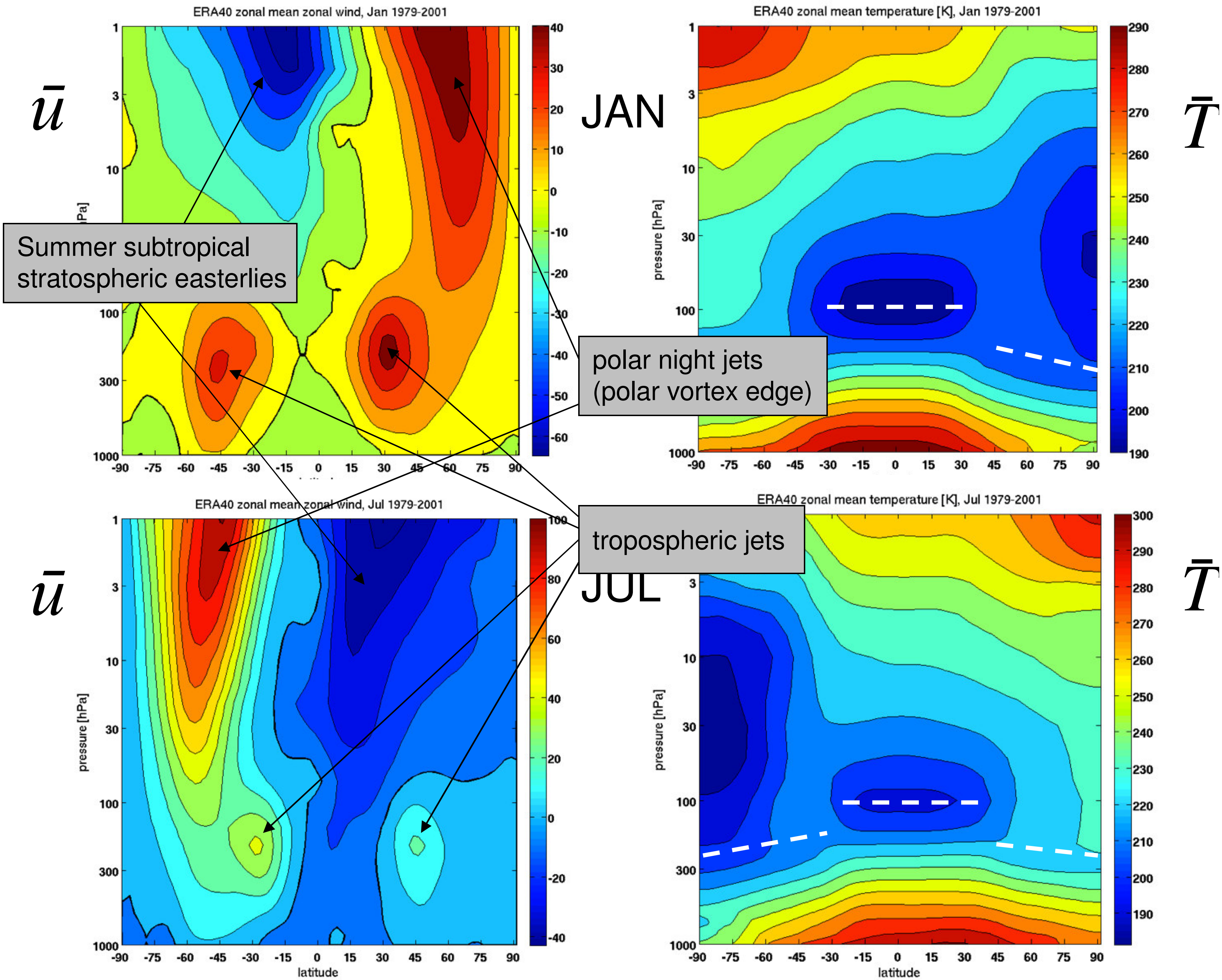

ERA40 zonal mean zonal wind, Jan 1979-2001
ERA40 zonal mean temperature [K], Jan 1979-2001
ERA40 zonal mean zonal wind, Jul 1979-2001
ERA40 zonal mean temperature [K], Jul 1979-2001
$\bar{u}$
$\bar{T}$
JAN
JUL
Summer subtropical stratospheric easterlies
polar night jets (polar vortex edge)
tropospheric jets
pressure [hPa]
latitude

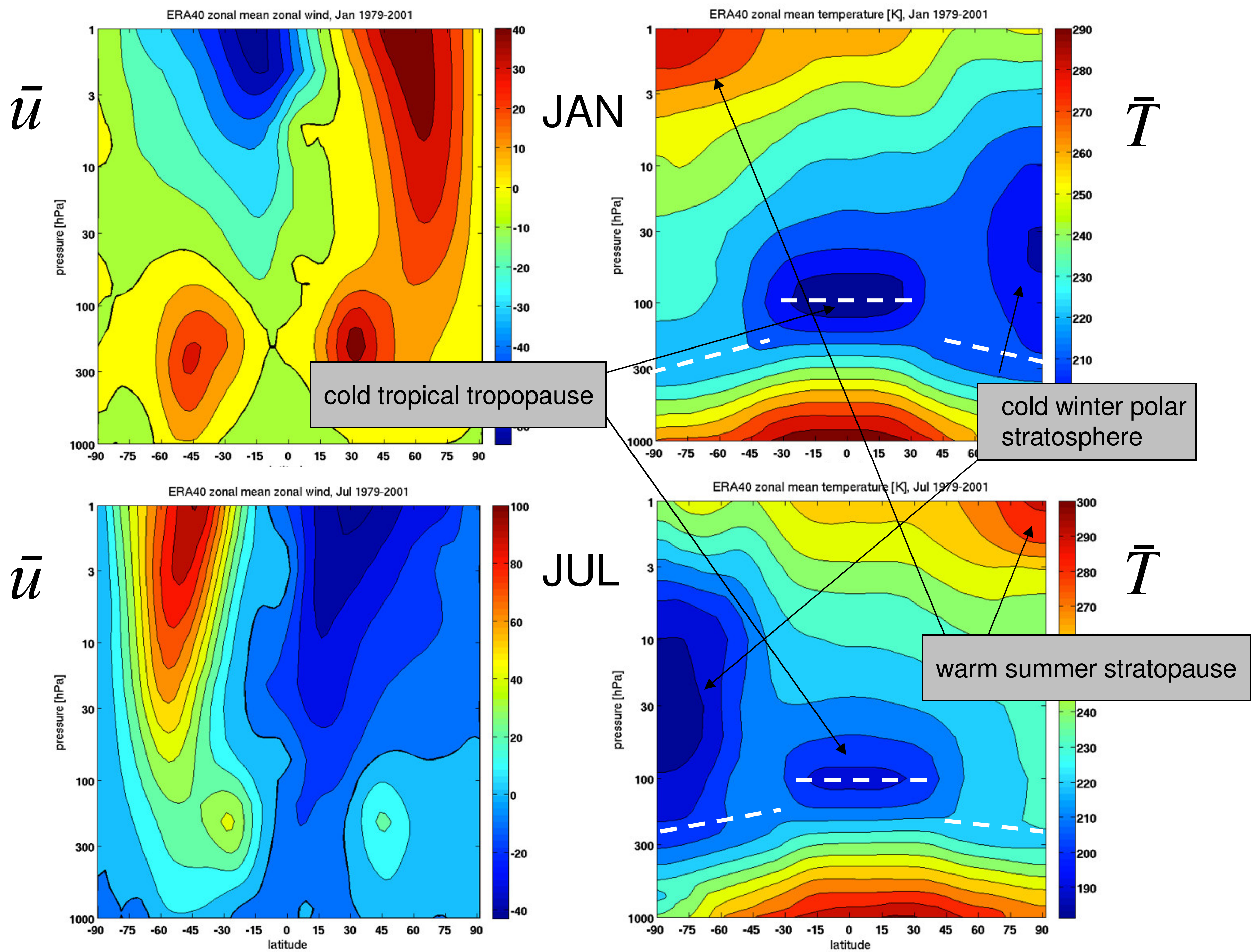

ERA40 zonal mean zonal wind, Jan 1979-2001
ERA40 zonal mean temperature [K], Jan 1979-2001
ERA40 zonal mean zonal wind, Jul 1979-2001
ERA40 zonal mean temperature [K], Jul 1979-2001
$\bar{u}$
$\bar{T}$
JAN
JUL
pressure [hPa]
latitude
cold tropical tropopause
cold winter polar stratosphere
warm summer stratopause

cold summer mesopause

warm winter mesopause

$\bar{T}$

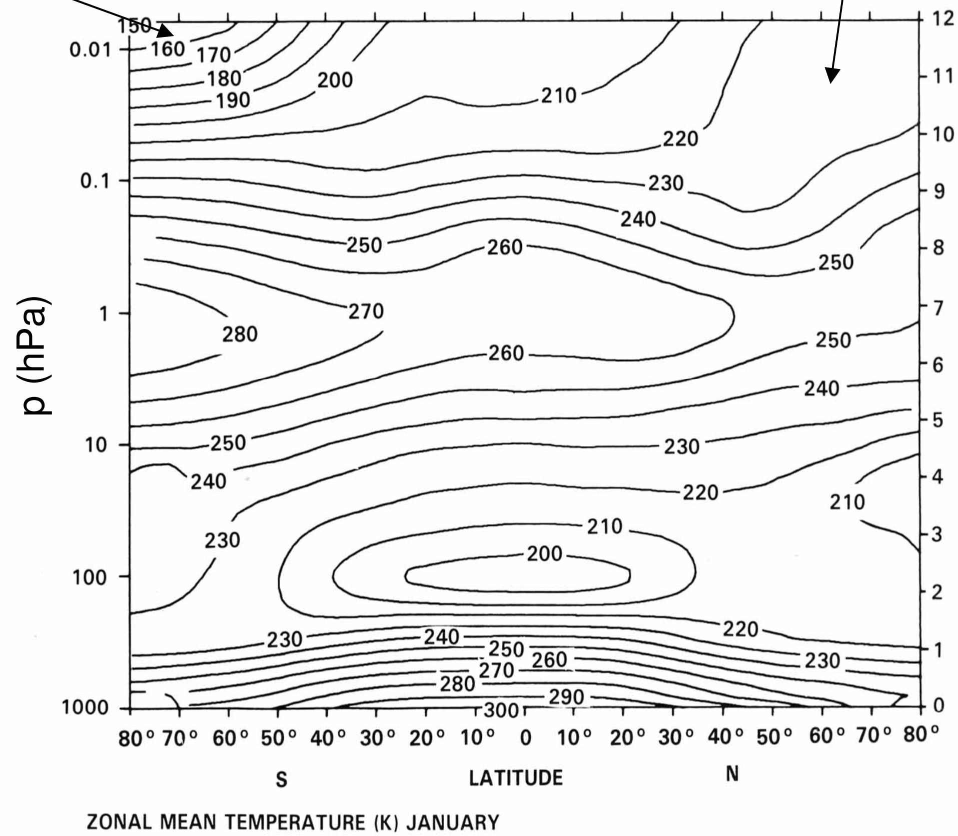

Figure 6-1. Cross sections [pressure (mbar)-latitude] of zonal mean temperature (K) for the average over 5 years of the monthly means for January. The data are from the combined SCR/PMR retrieval made at the University of Oxford for the period January 1973 to December 1974 and July 1975 to June 1978. (Supplied by J.J. Barnett and M. Corney).

Radiative-convective equilibrium (no large-scale heat transport)

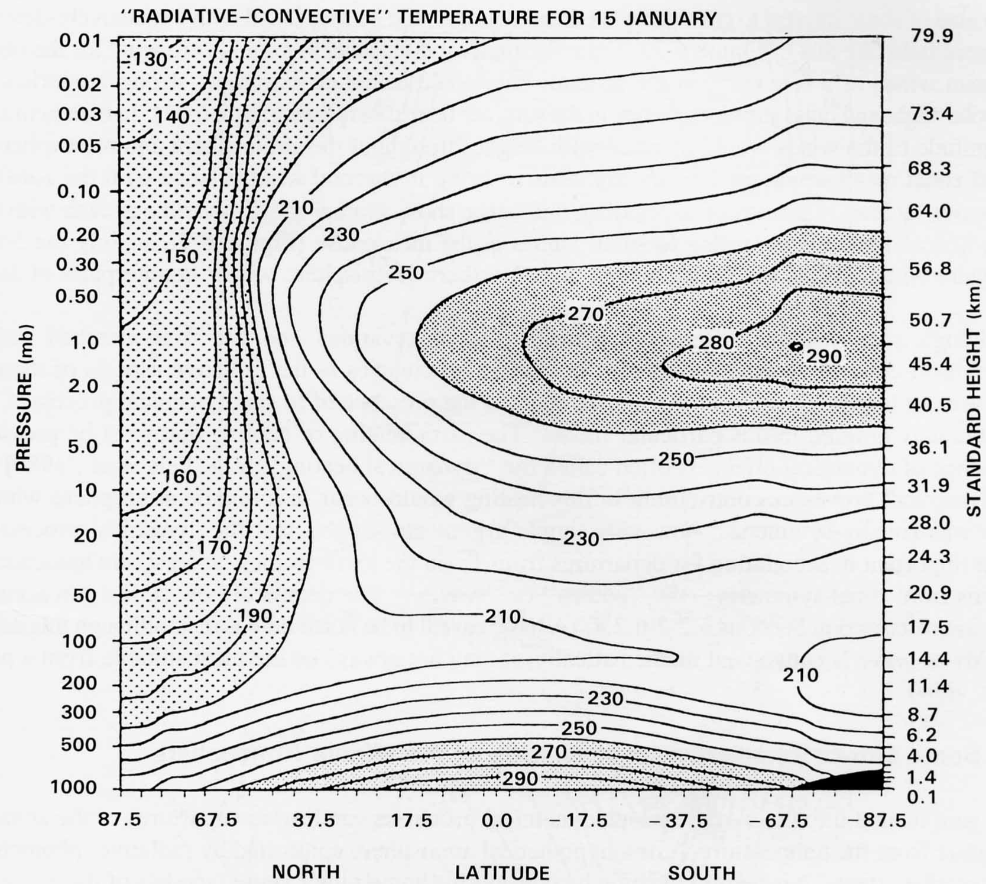

Figure 6-30. Time-dependent ''radiatively-determined'' temperature T_r for 15 January 1982 from the calculation of Fels and Schwarzkopf (1985). The surface temperatures are prescribed at their seasonally-varying observed values. Cloudiness, and ozone below 35 km, are prescribed at annual-mean values, as in Fels *et al.* (1980); ozone above 35 km is allowed to ''float'', in response to temperature variations, towards a crude photochemical equilibrium. Details of the water vapor prescription are relatively standard and are described in Fels and Schwarzkopf (1985). [From Mahlman and Umscheid, 1984].

January

$\bar{T}$ T_e

ZONAL MEAN WIND (m/s)

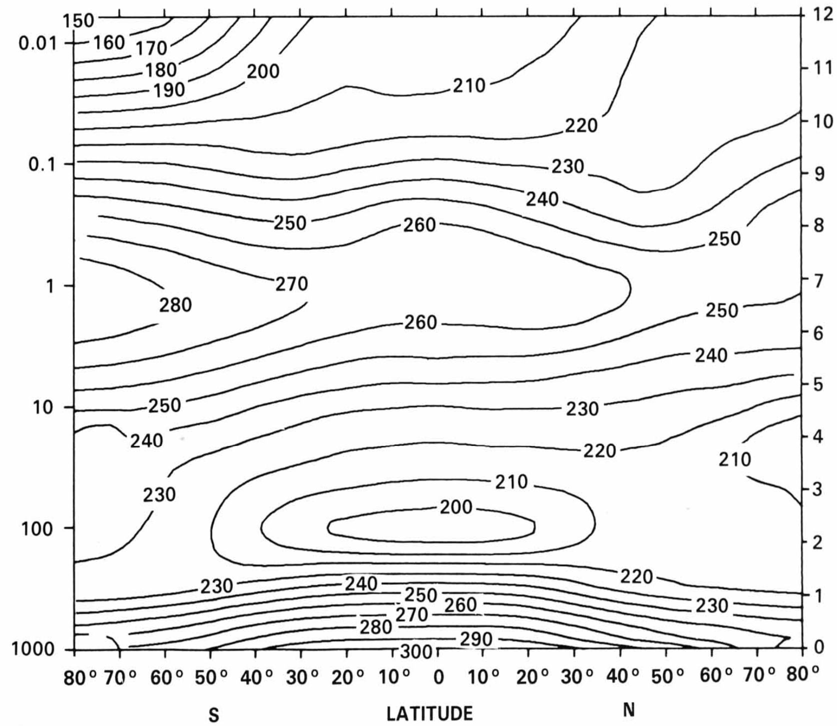

ZONAL MEAN TEMPERATURE (K) JANUARY

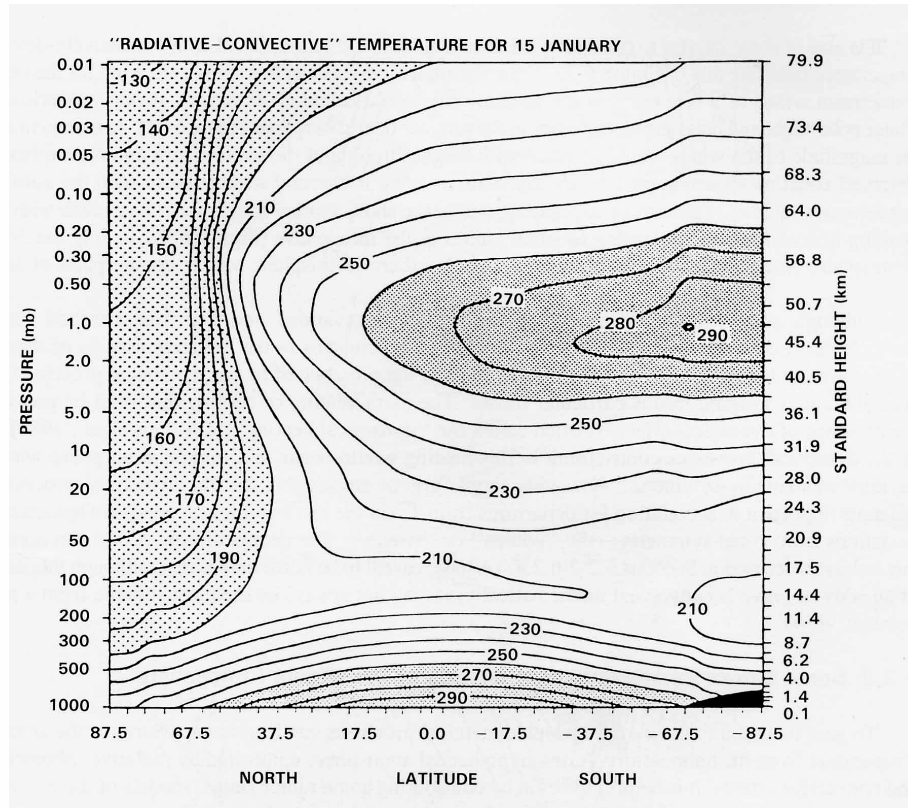

$$\bar{w}_* \frac{\partial \theta}{\partial z} = \frac{1}{\rho \Pi} \bar{J} = -\left(\frac{c_p}{\Pi}\right) \frac{1}{\tau_{rad}} (\bar{T} - T_e)$$

$$\rightarrow \quad \bar{w}_* \left(\frac{\partial \bar{T}}{\partial z} + \frac{\kappa}{H} \bar{T}\right) = -\frac{1}{\tau_{rad}} (\bar{T} - T_e)$$

$$\left(\frac{\partial \bar{T}}{\partial z} + \frac{\kappa}{H} \bar{T} \simeq 10 \text{ K km}^{-1}\right)$$

$\bar{T}$ $\qquad\qquad$ T_e

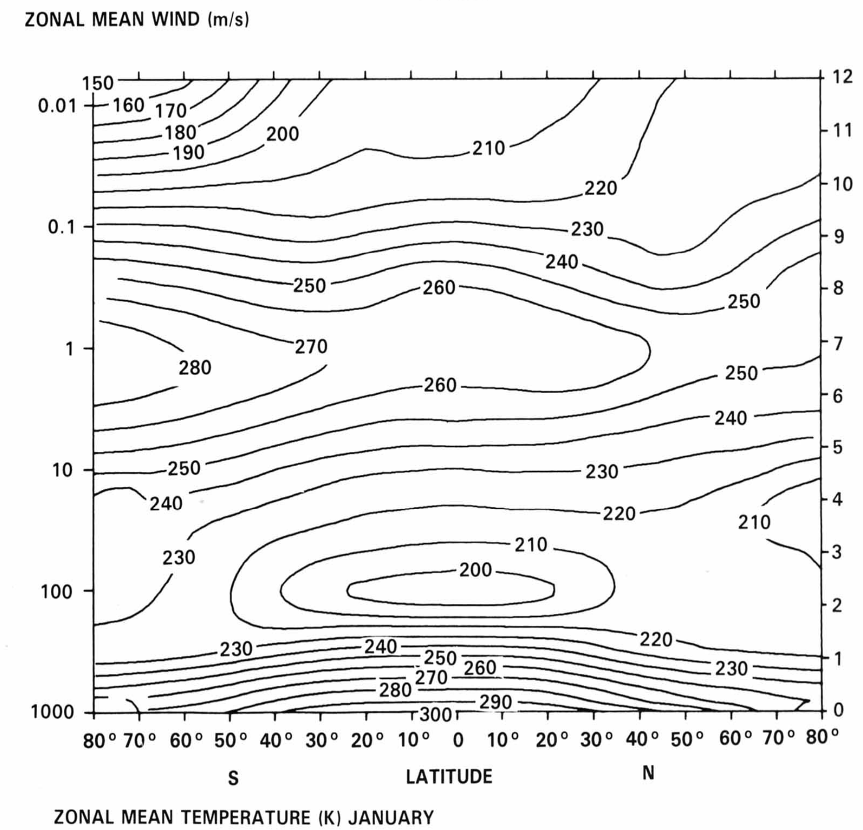

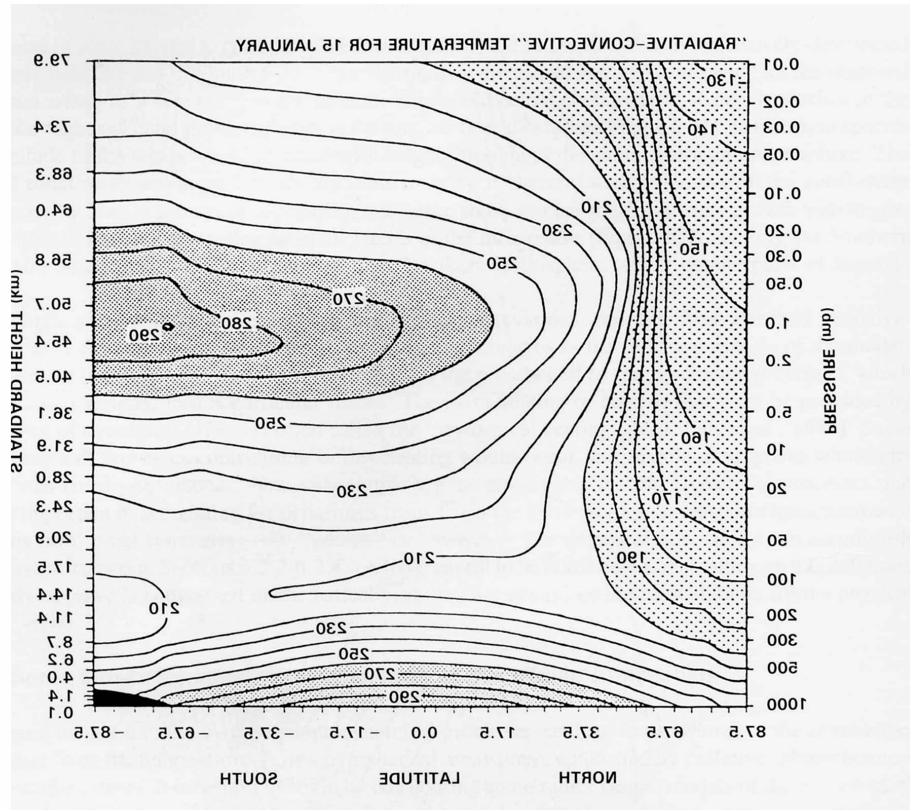

$$\bar{w}_* \frac{\partial \theta}{\partial z} = \frac{1}{\rho \Pi} \bar{J} = -\left(\frac{c_p}{\Pi}\right) \frac{1}{\tau_{rad}} (\bar{T} - T_e)$$

$$\rightarrow \qquad \bar{w}_* \left(\frac{\partial \bar{T}}{\partial z} + \frac{\kappa}{H} \bar{T}\right) = -\frac{1}{\tau_{rad}} (\bar{T} - T_e)$$

$$\left(\frac{\partial \bar{T}}{\partial z} + \frac{\kappa}{H} \bar{T} \simeq 10 \text{ K km}^{-1}\right)$$

$\bar{T}$ $\qquad\qquad\qquad$ T_e

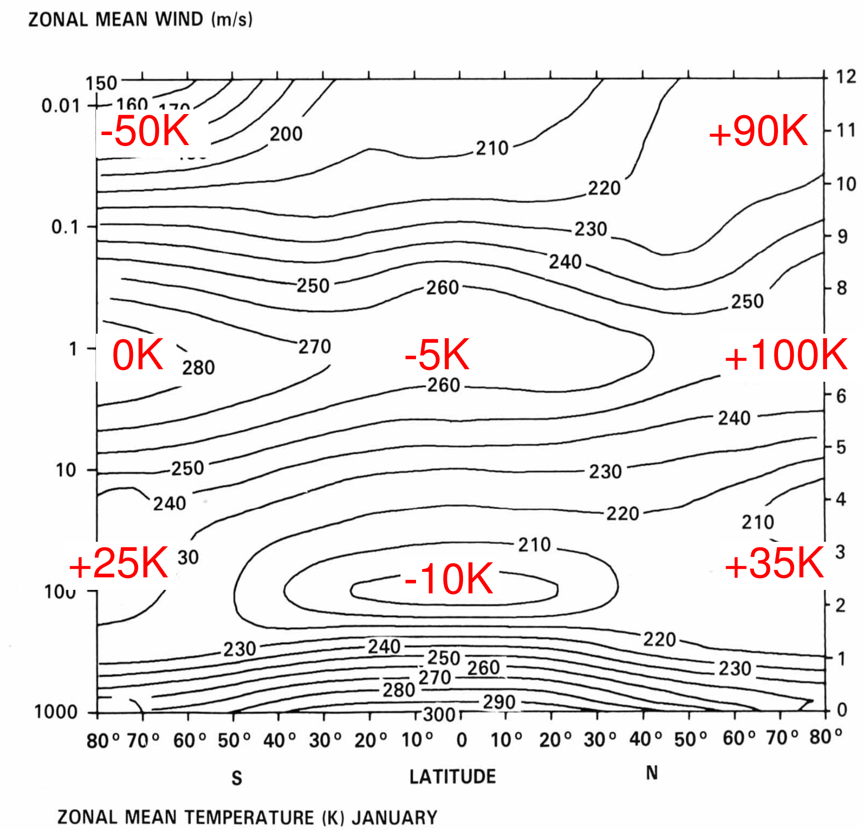

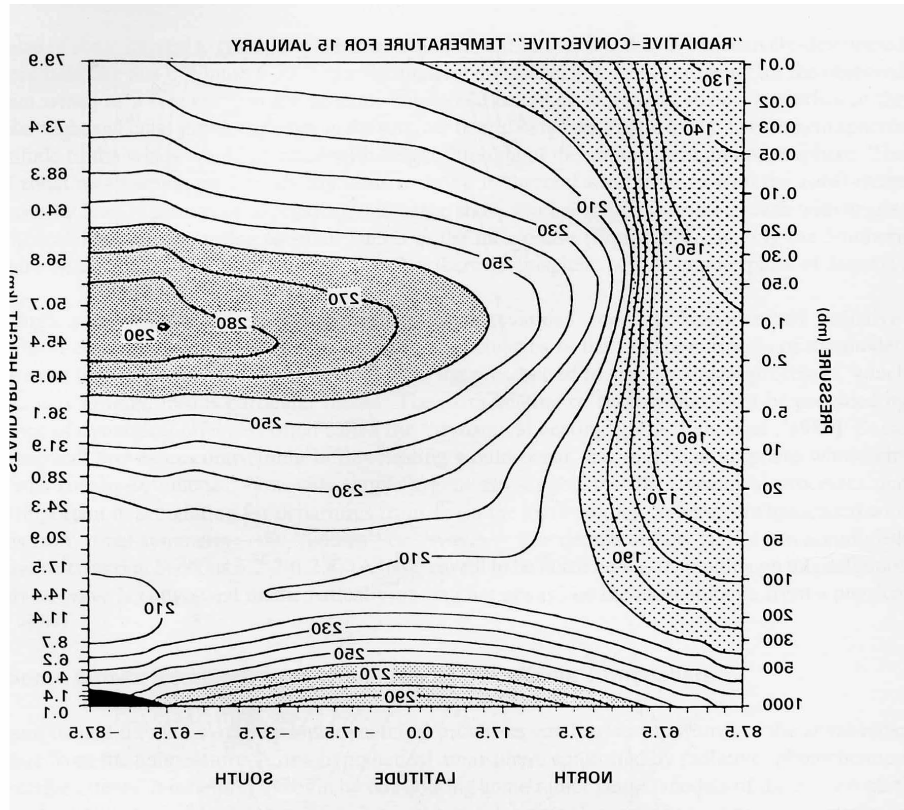

$$\bar{w}_* \frac{\partial \theta}{\partial z} = \frac{1}{\rho \Pi} \bar{J} = -\left(\frac{c_p}{\Pi}\right) \frac{1}{\tau_{rad}} (\bar{T} - T_e)$$

$$\rightarrow \qquad \bar{w}_* \left(\frac{\partial \bar{T}}{\partial z} + \frac{\kappa}{H} \bar{T}\right) = -\frac{1}{\tau_{rad}} \boxed{(\bar{T} - T_e)}$$

$$\left(\frac{\partial \bar{T}}{\partial z} + \frac{\kappa}{H} \bar{T} \simeq 10 \text{ K km}^{-1}\right)$$

$\bar{T}$ T_e

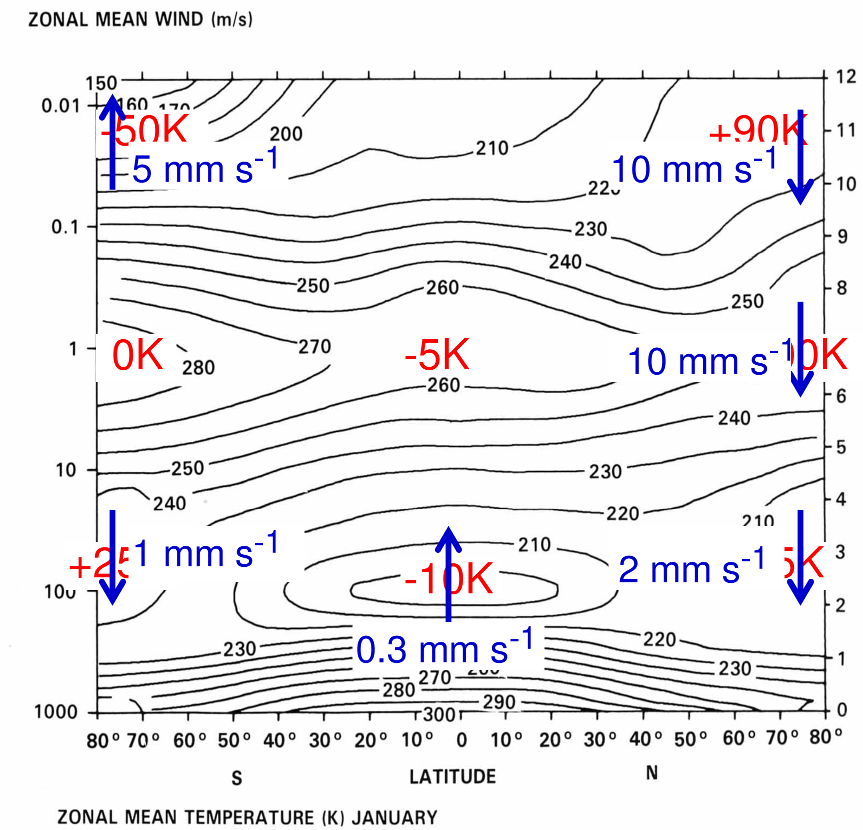

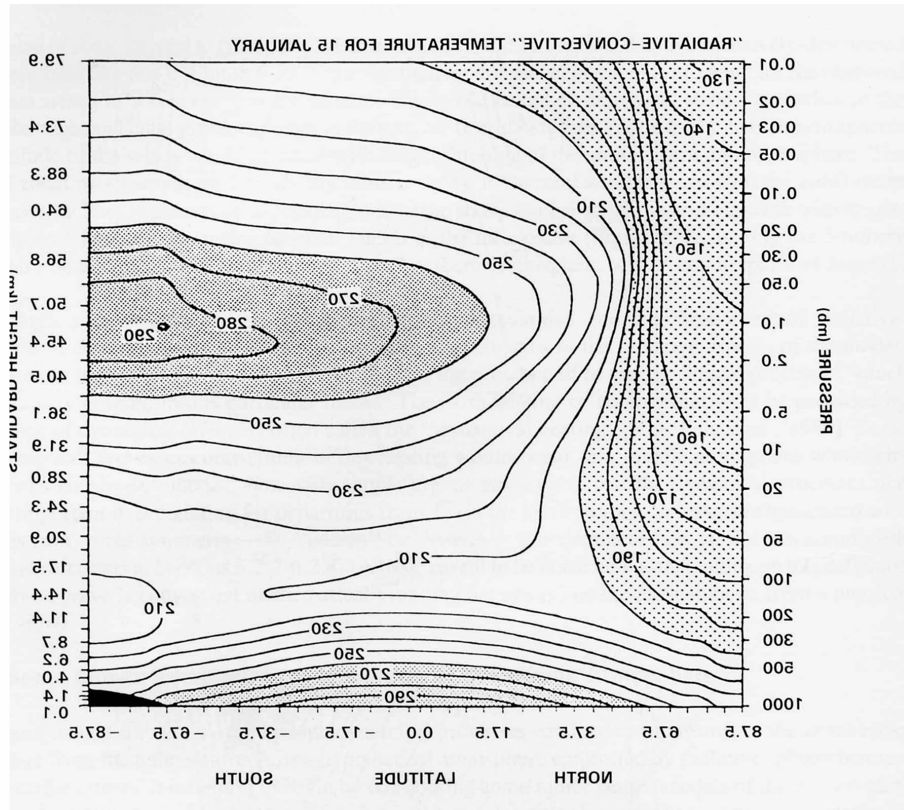

$$\bar{w}_* \frac{\partial \theta}{\partial z} = \frac{1}{\rho \Pi} \bar{J} = -\left(\frac{c_p}{\Pi}\right) \frac{1}{\tau_{rad}} (\bar{T} - T_e)$$

$$\rightarrow \quad \boxed{\bar{w}_*} \left(\frac{\partial \bar{T}}{\partial z} + \frac{\kappa}{H} \bar{T}\right) = -\frac{1}{\tau_{rad}} (\bar{T} - T_e)$$

$$\left(\frac{\partial \bar{T}}{\partial z} + \frac{\kappa}{H} \bar{T} \simeq 10 \text{ K km}^{-1}\right)$$

$\bar{T}$

$$\frac{1}{a\cos\varphi}\frac{\partial}{\partial\varphi}(\bar{v}_*\cos\varphi) + \frac{1}{\rho}\frac{\partial}{\partial z}(\rho\bar{w}_*) = 0$$

T_e

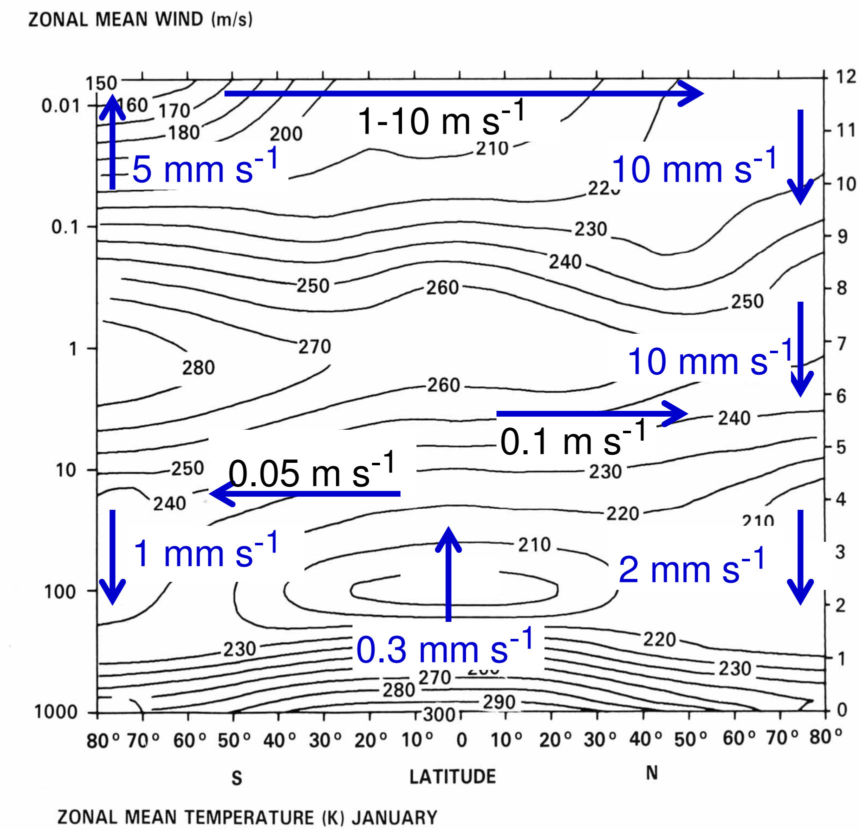

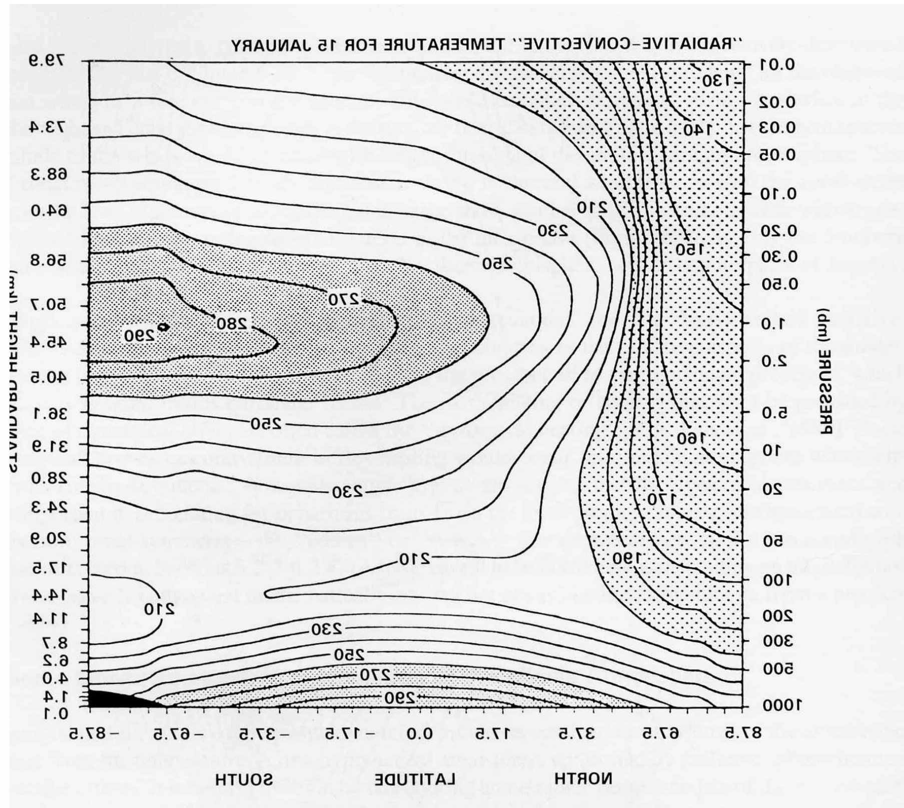

$$\bar{w}_*\frac{\partial\theta}{\partial z} = \frac{1}{\rho\Pi}\bar{J} = -\left(\frac{c_p}{\Pi}\right)\frac{1}{\tau_{rad}}(\bar{T} - T_e)$$

$$\rightarrow \quad \bar{w}_*\left(\frac{\partial\bar{T}}{\partial z} + \frac{\kappa}{H}\bar{T}\right) = -\frac{1}{\tau_{rad}}(\bar{T} - T_e)$$

$$\left(\frac{\partial\bar{T}}{\partial z} + \frac{\kappa}{H}\bar{T} \simeq 10\text{ K km}^{-1}\right)$$

Residual circulation diagnosed from satellite-derived temperatures and radiation budget

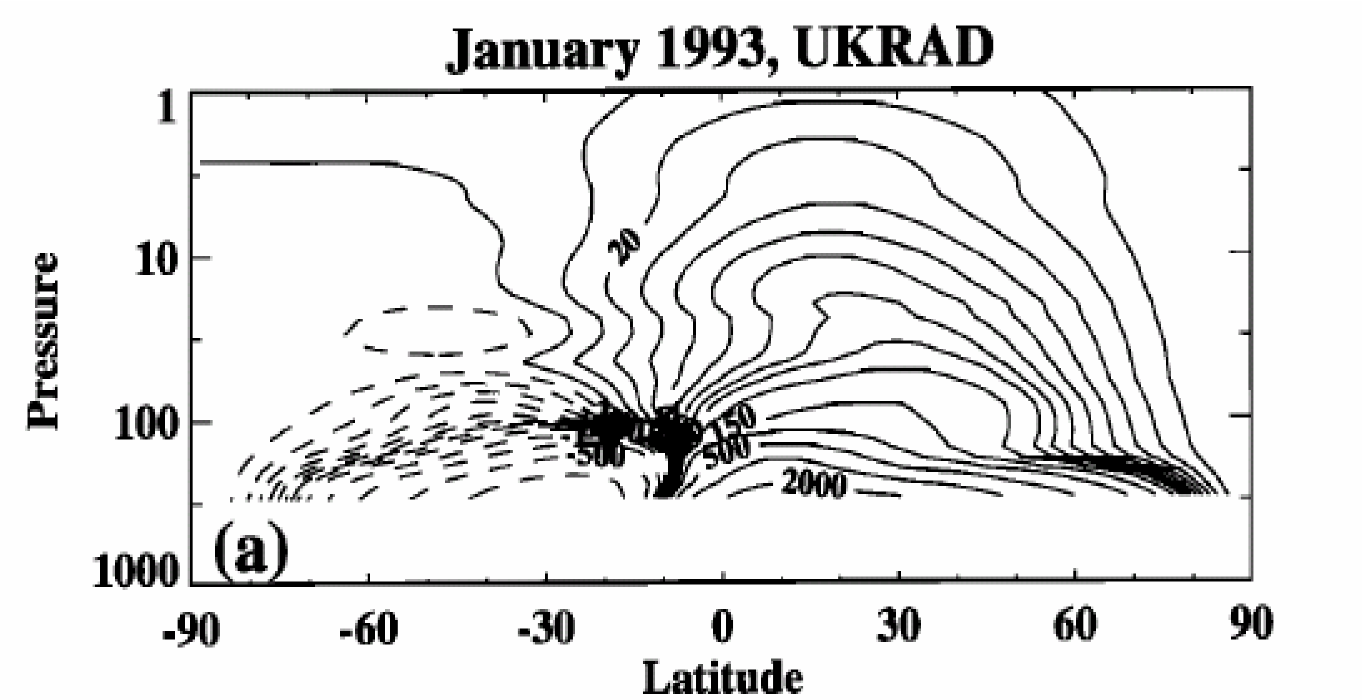

[Rosenlof, *J Geophys Res*, 1995]

(ii) Stratospheric Rossby waves

Planetary-scale Rossby waves in winter
(spring in southern hemisphere)

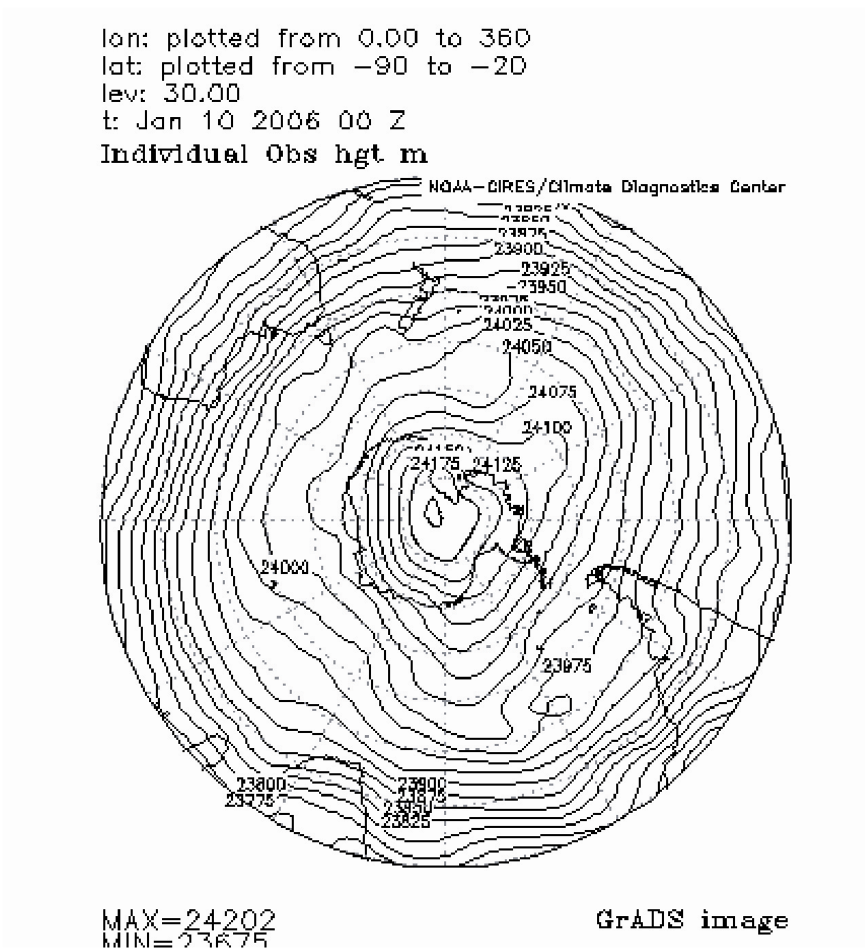

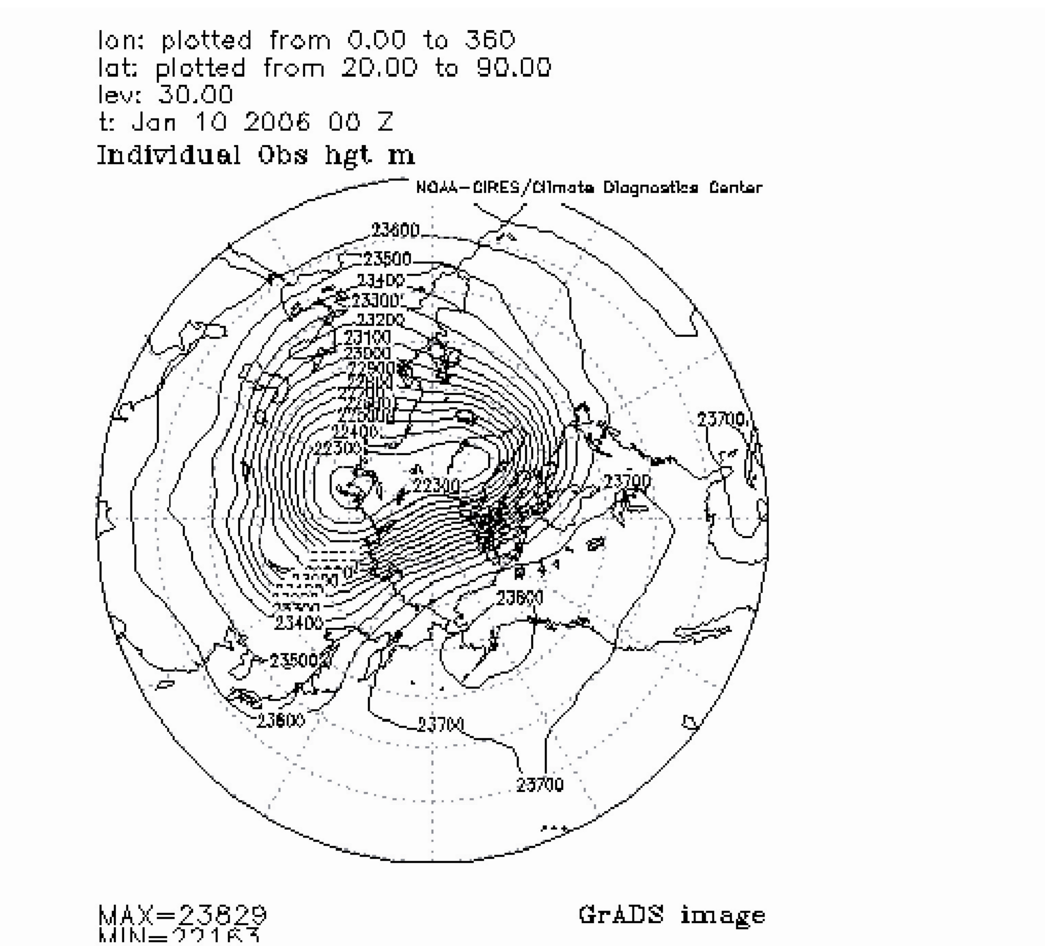

2006 January 10

Geopotential height (m)

100 hPa

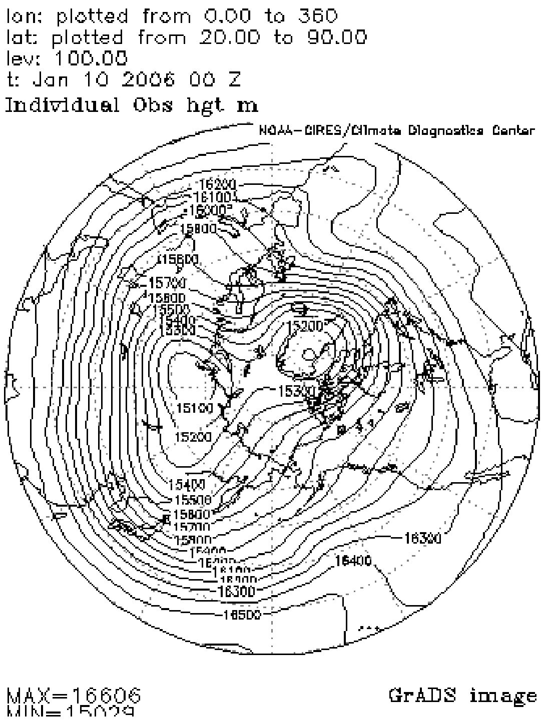

30hPa

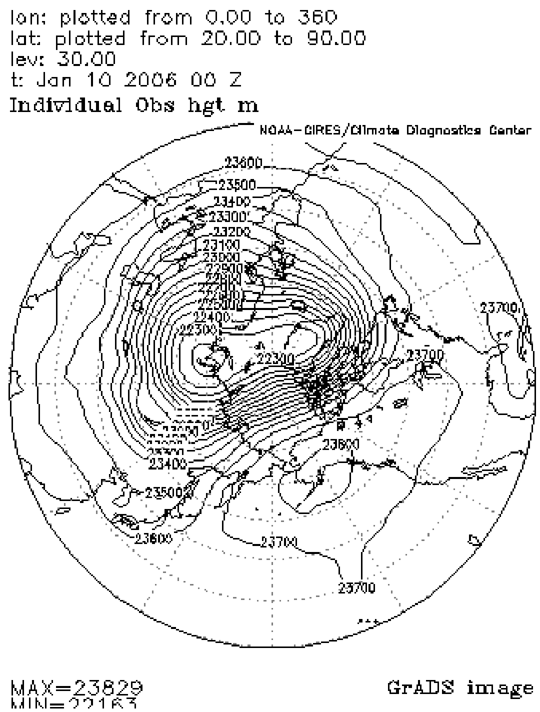

10hPa

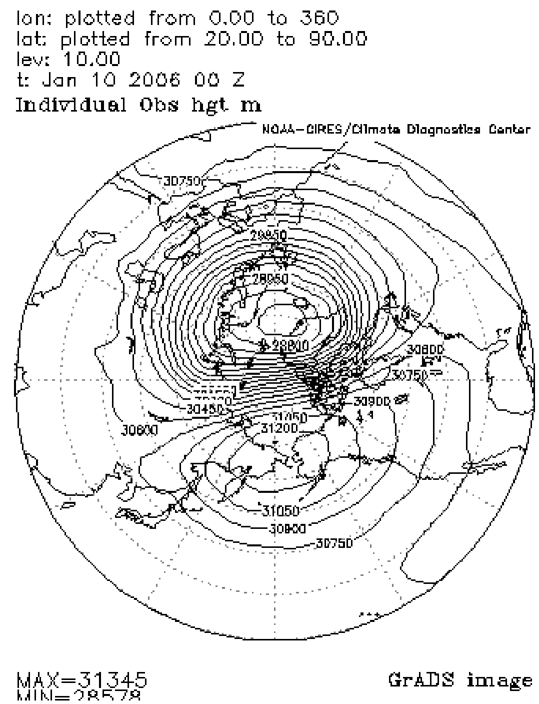

Wave breaking in the stratosphere

Ertel PV $g^{-1}\frac{\partial\theta}{\partial p}(f+\zeta)$

conserved in adiabatic flow

850K

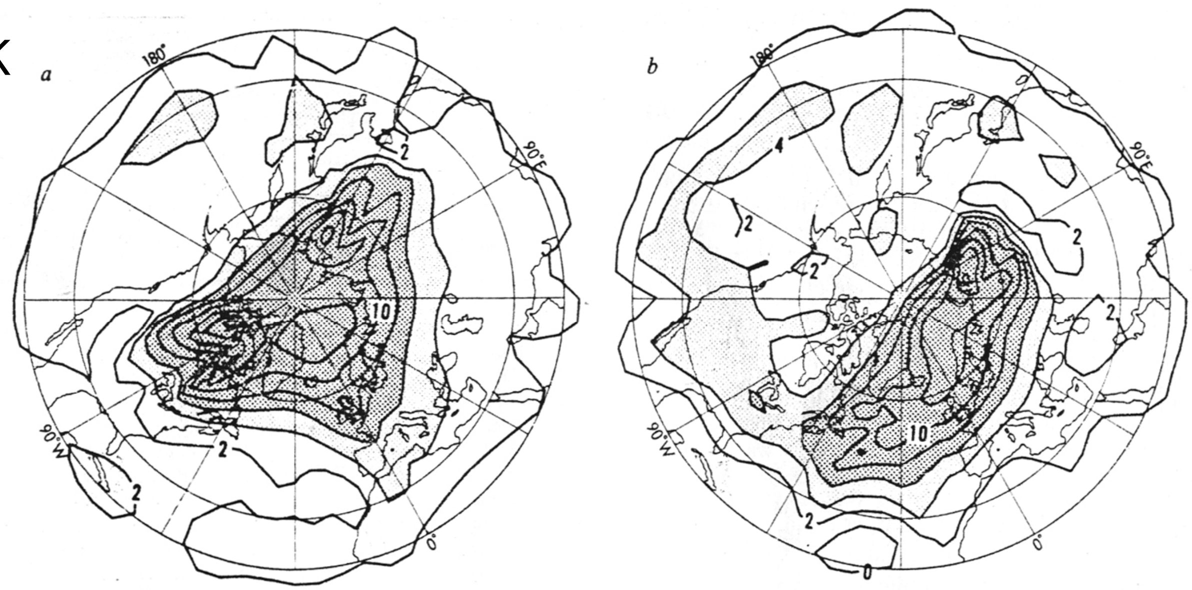

Fig. 2 Coarse-grain estimates of Ertel's potential vorticity Q on the 850 K isentropic surface (near the 10-mbar isobaric surface) on 17 (*a*) and 27 (*b*) January 1979, at 00 h GMT. The southernmost latitude circle shown is 20° N; the others are 30° N and 60° N. Map projection is polar stereographic. For units see equation (5) onwards. Contour interval is 2 units. Values greater than 4 units are lightly shaded, and greater than 6 units heavily shaded.

[McIntyre & Palmer, *Nature, 1983]*

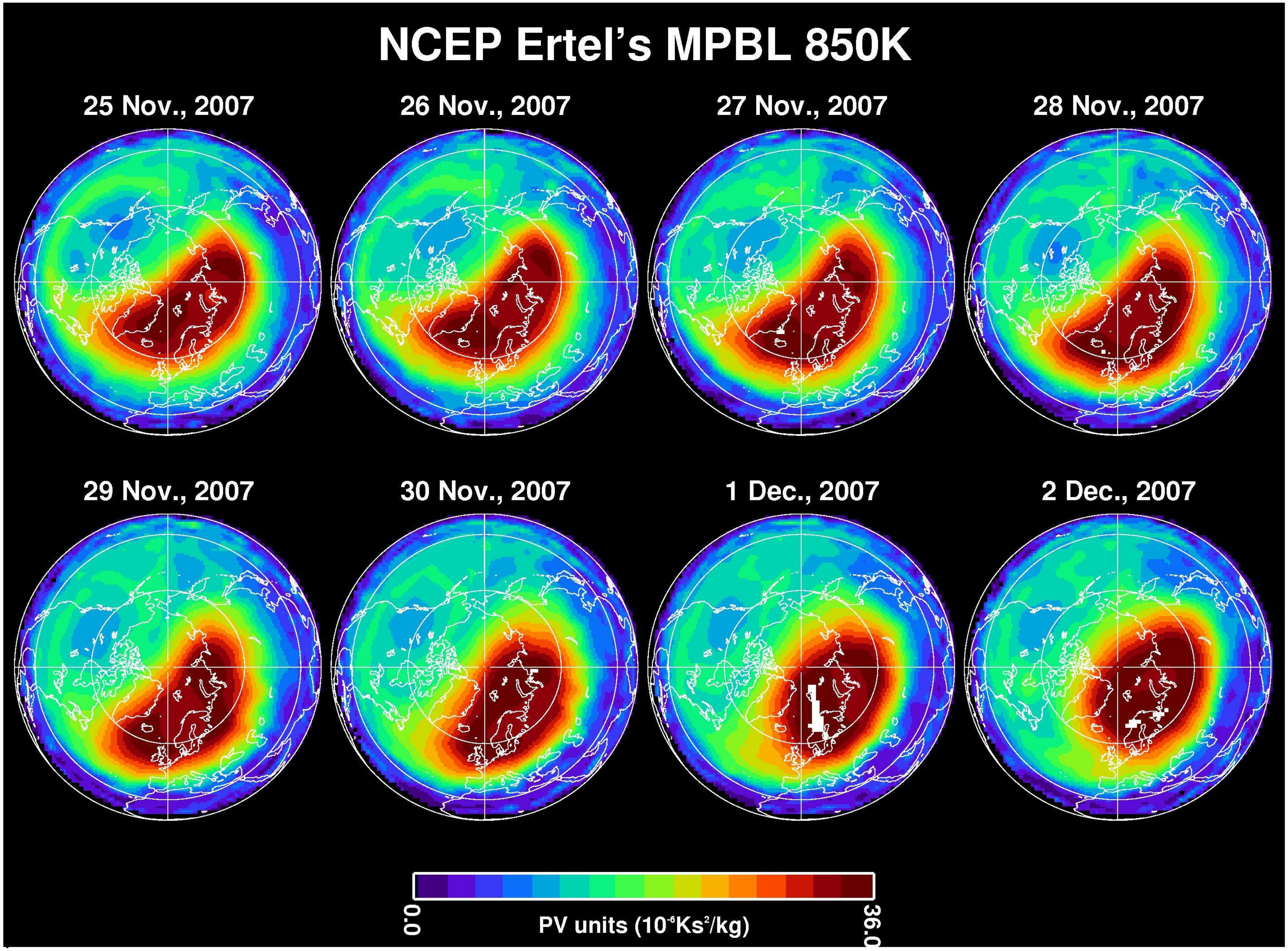
NCEP Ertel's MPBL 850K
25 Nov., 2007
26 Nov., 2007
27 Nov., 2007
28 Nov., 2007
29 Nov., 2007
30 Nov., 2007
1 Dec., 2007
2 Dec., 2007
0.0
PV units (10-6Ks2/kg)
36.0

1992 September 6

southern hemisphere
middle stratosphere

10 hPa

geopotential
height (m)

10 hPa

radiative heating
(K day^{-1})

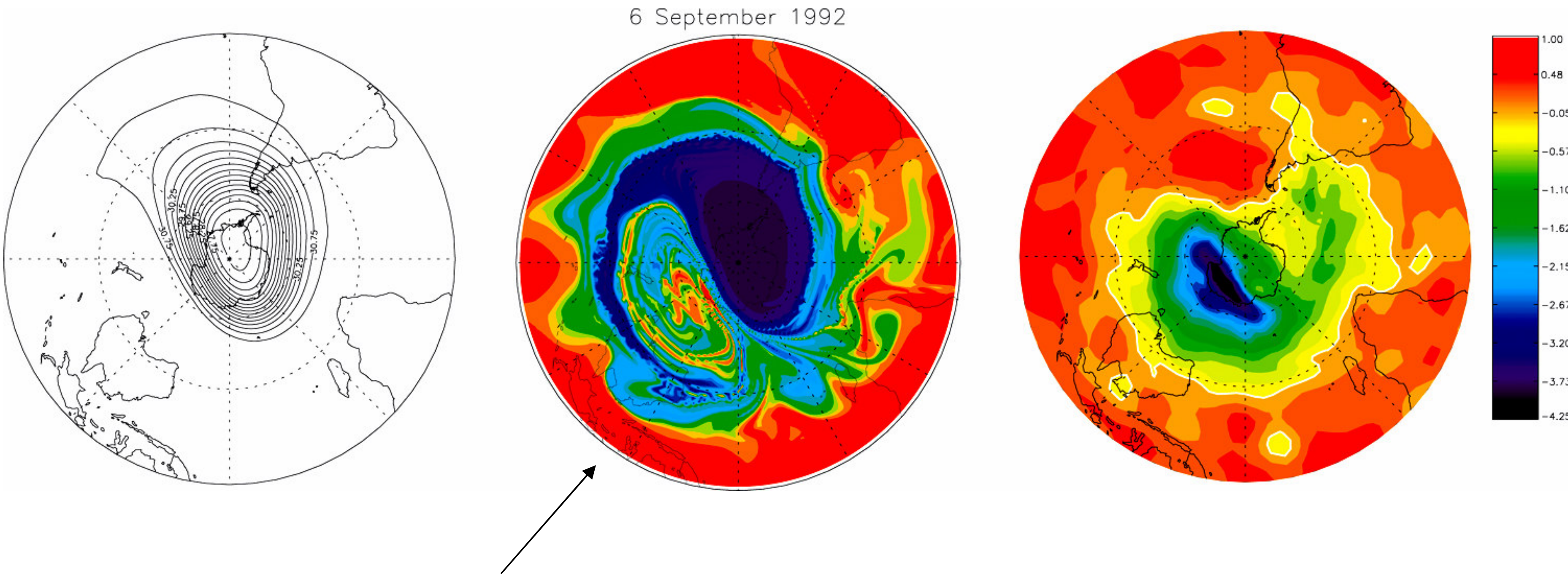

tracer advected with analyzed winds
for 10 days on 850K isentropic surface

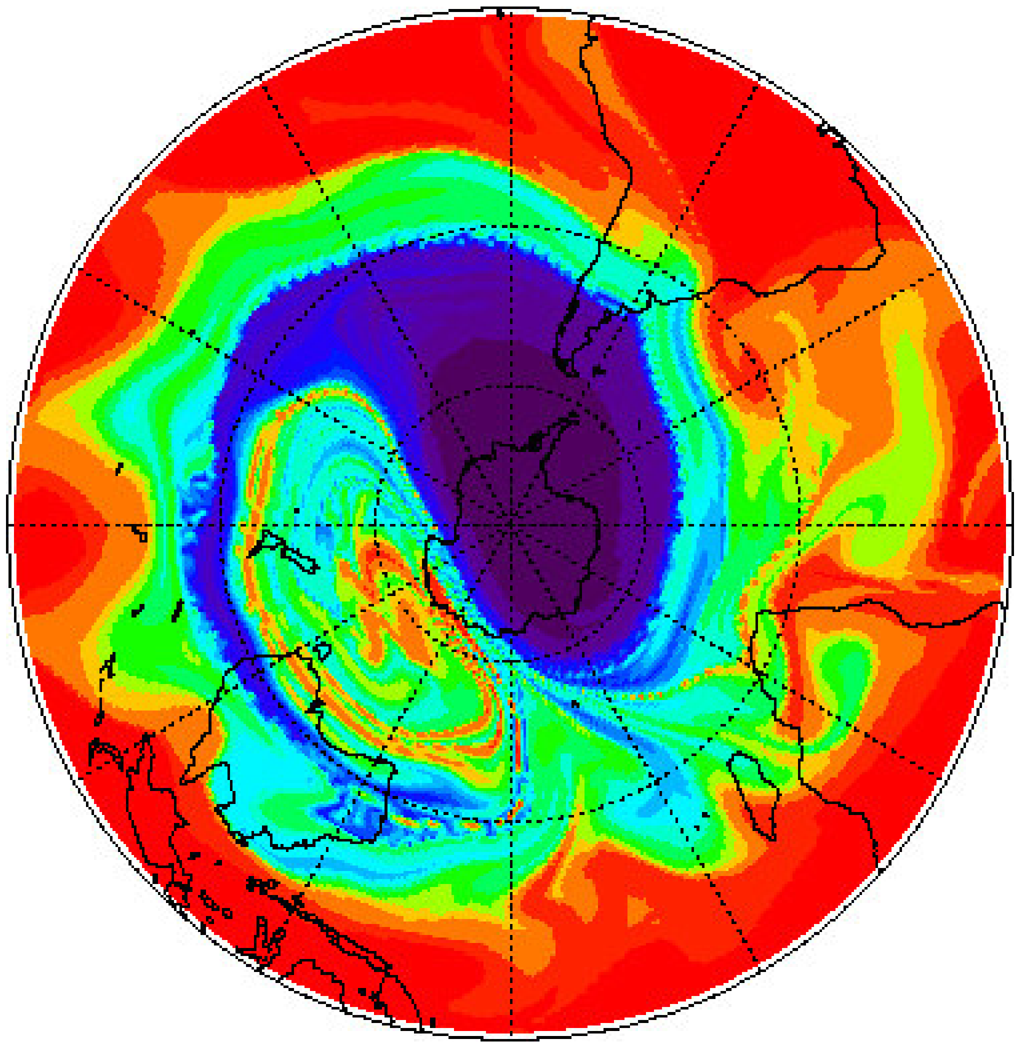

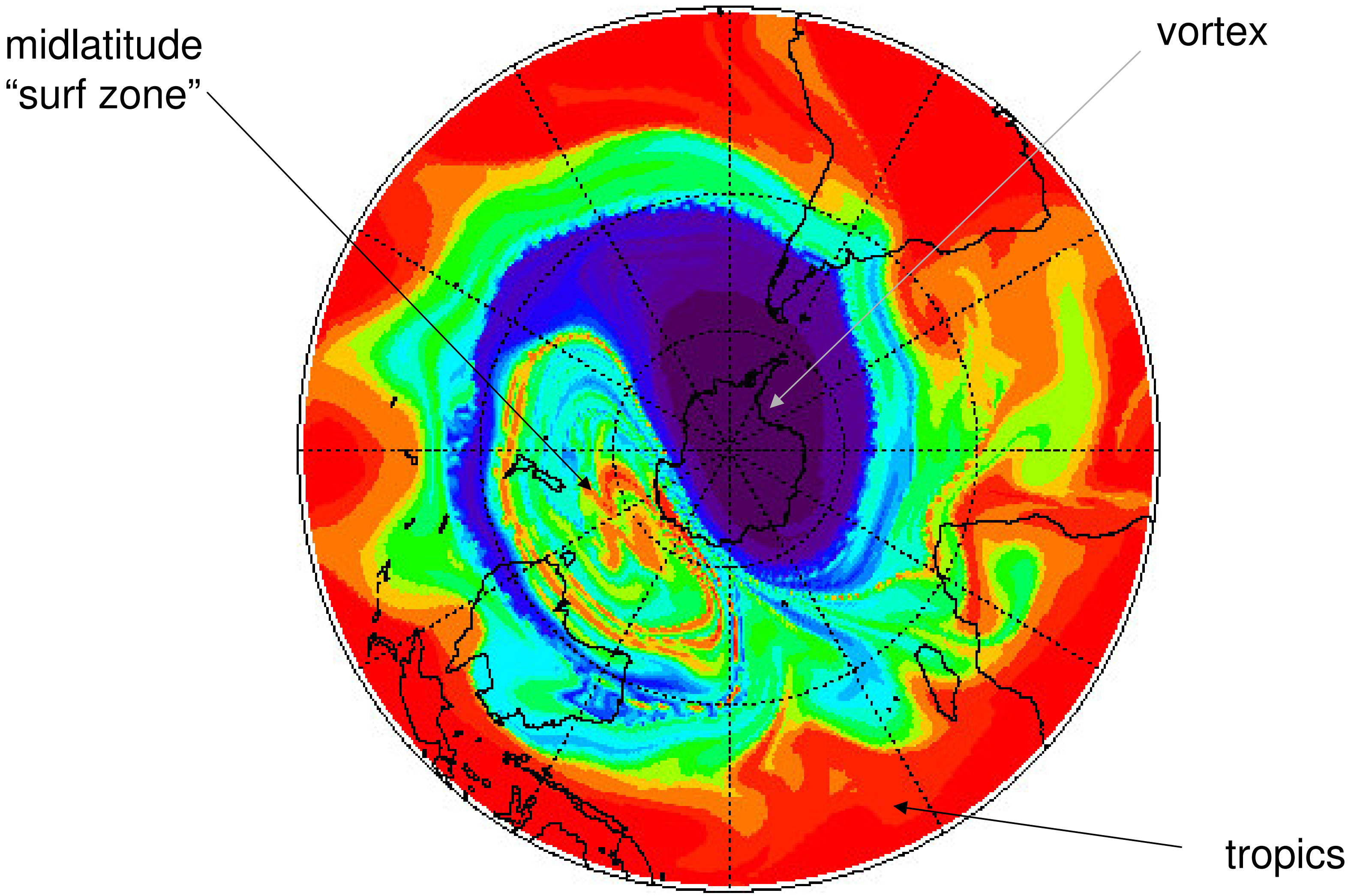
midlatitude
“surf zone”
vortex
tropics

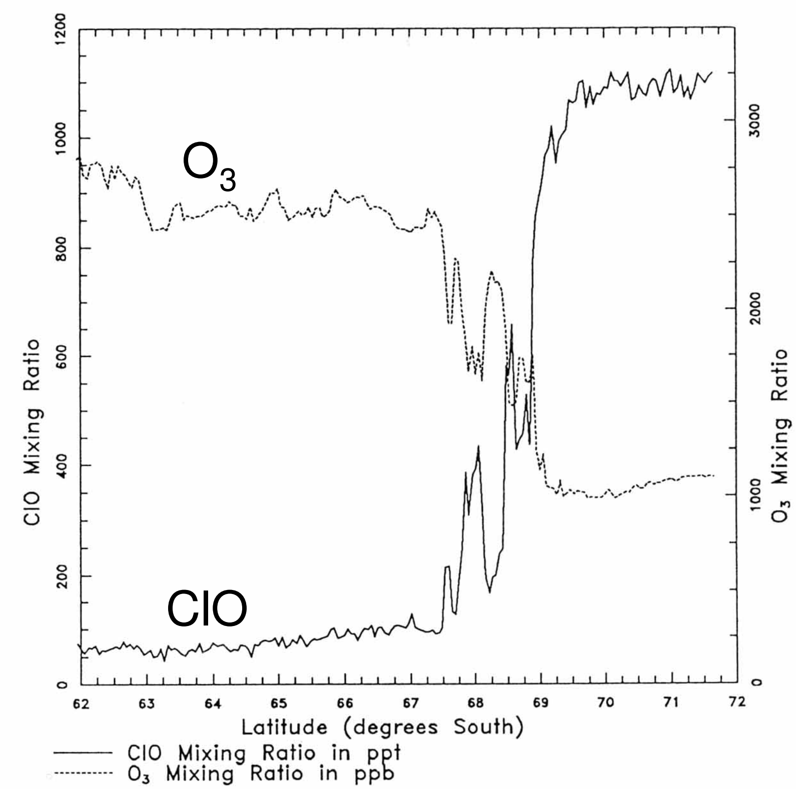

Fig. 14. Simultaneously observed ClO and O_3 obtained on September 16, 1987, by the ER-2, with corrections made for variations in potential temperature. Results shown here correspond to what the aircraft would have observed on a 450 K isentropic surface.

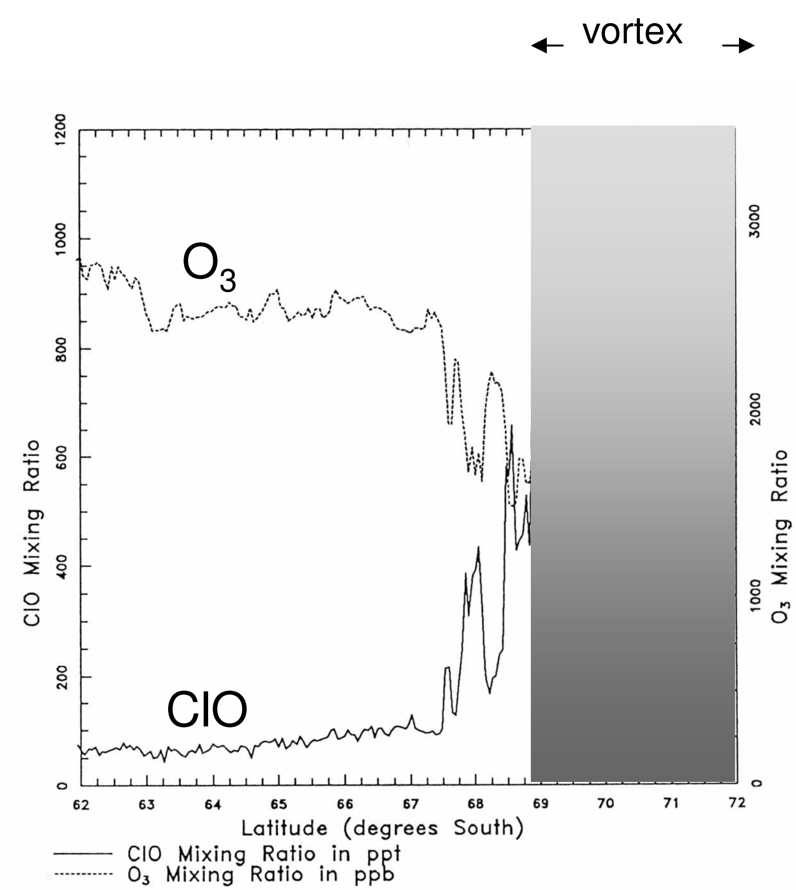

Fig. 14. Simultaneously observed ClO and O_3 obtained on September 16, 1987, by the ER-2, with corrections made for variations in potential temperature. Results shown here correspond to what the aircraft would have observed on a 450 K isentropic surface.

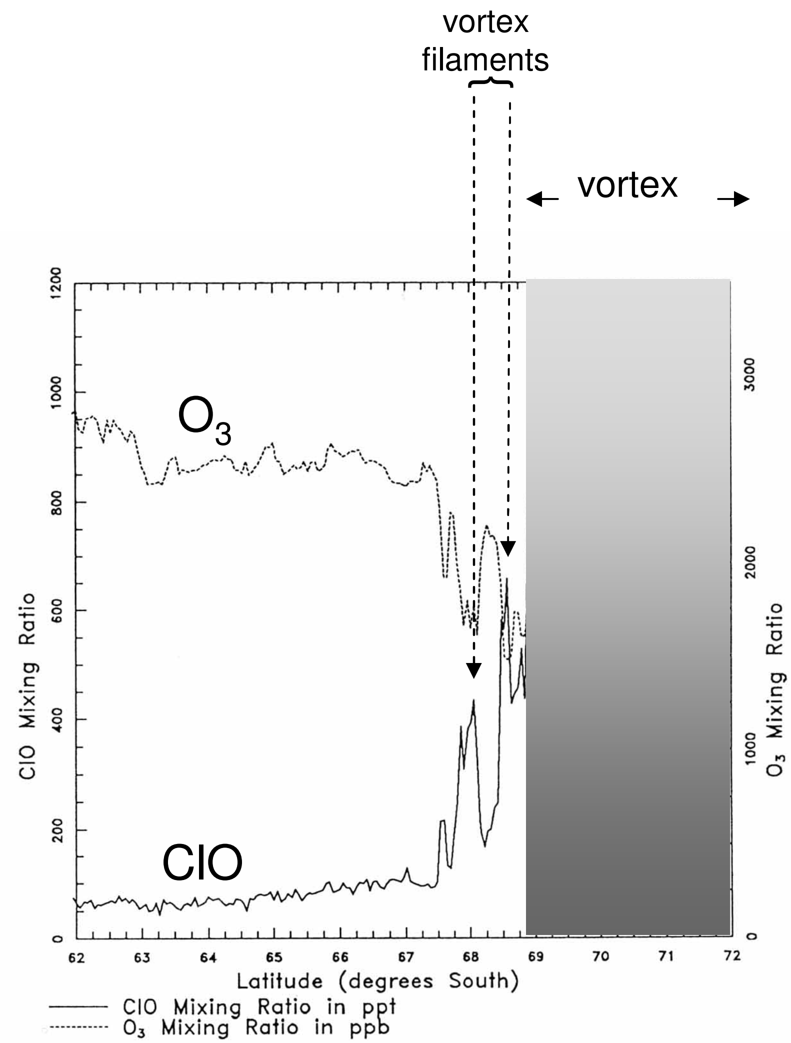

Fig. 14. Simultaneously observed ClO and O_3 obtained on September 16, 1987, by the ER-2, with corrections made for variations in potential temperature. Results shown here correspond to what the aircraft would have observed on a 450 K isentropic surface.

1992 January 28

50 hPa

geopotential height (m)

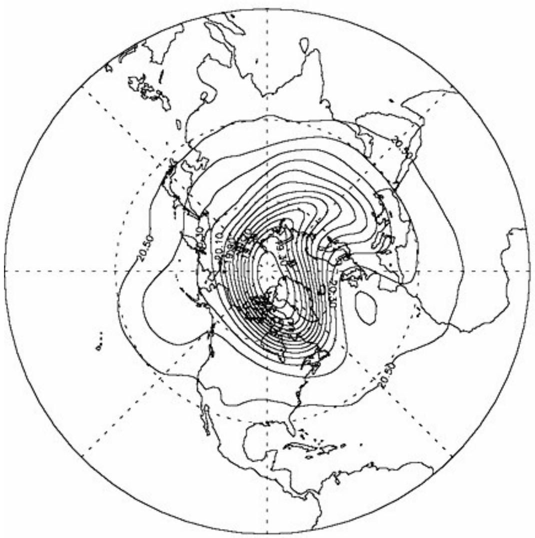

northern hemisphere lower stratosphere

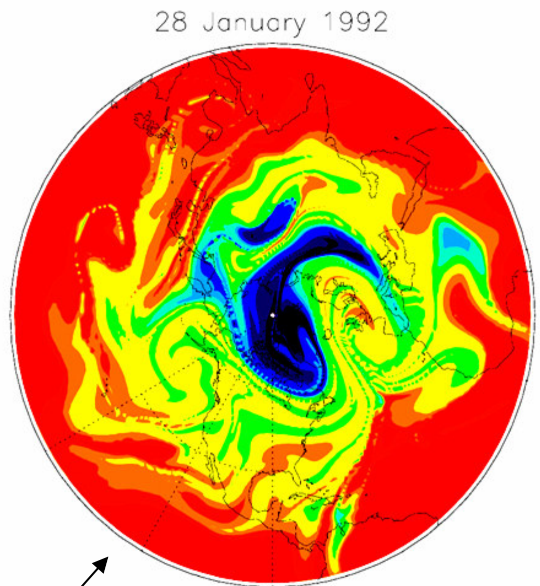

tracer advected with analyzed winds for 10 days on 480K isentropic surface

50 hPa

radiative heating ($K\ day^{-1}$)

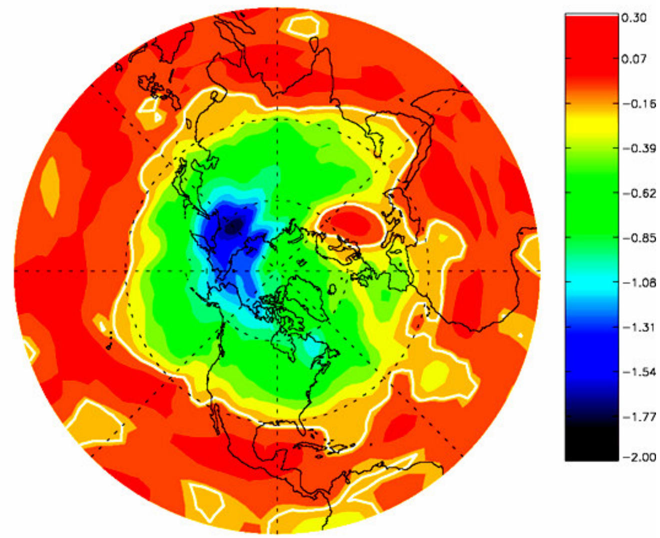

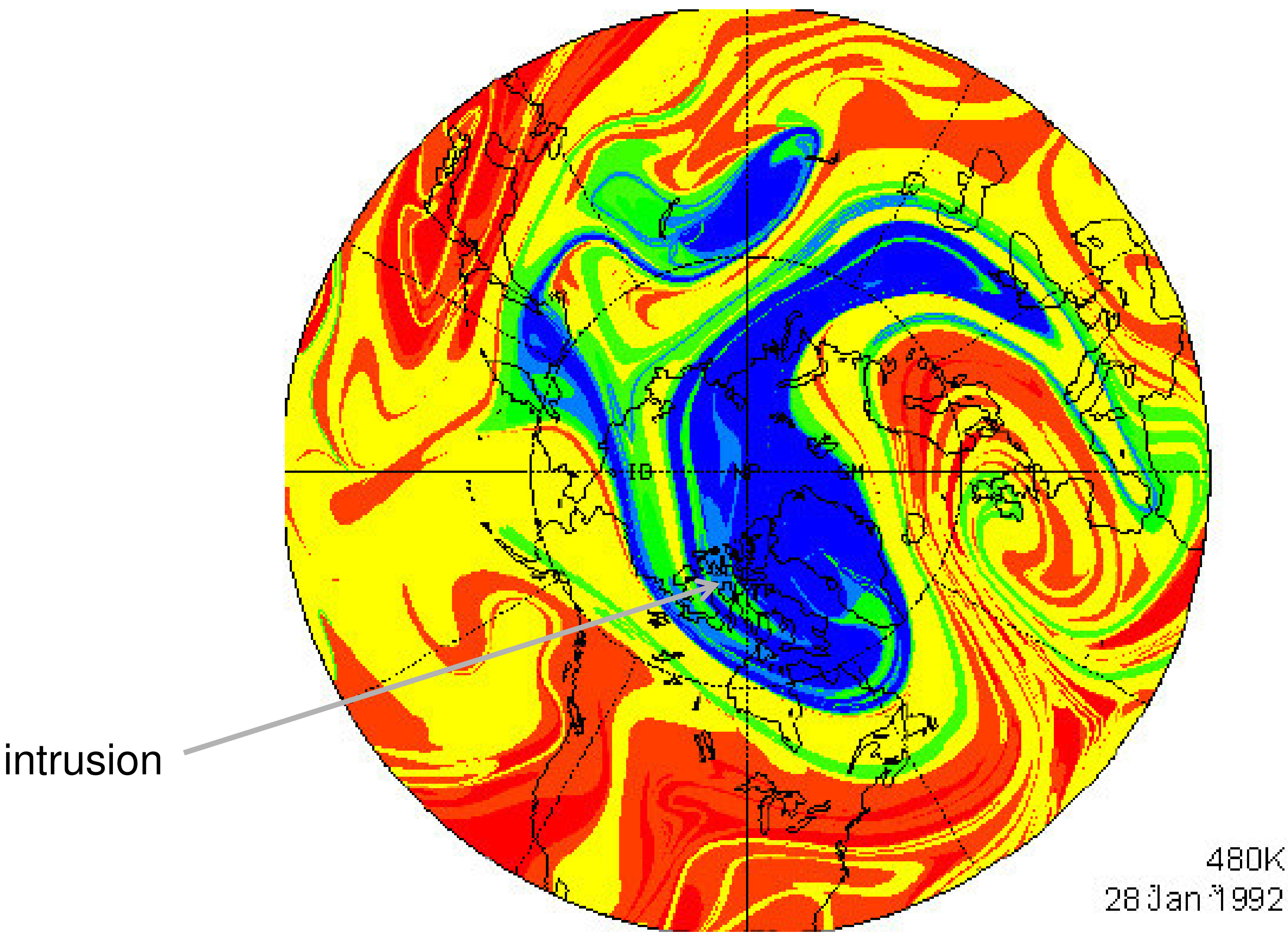
intrusion
480K
28 Jan 1992

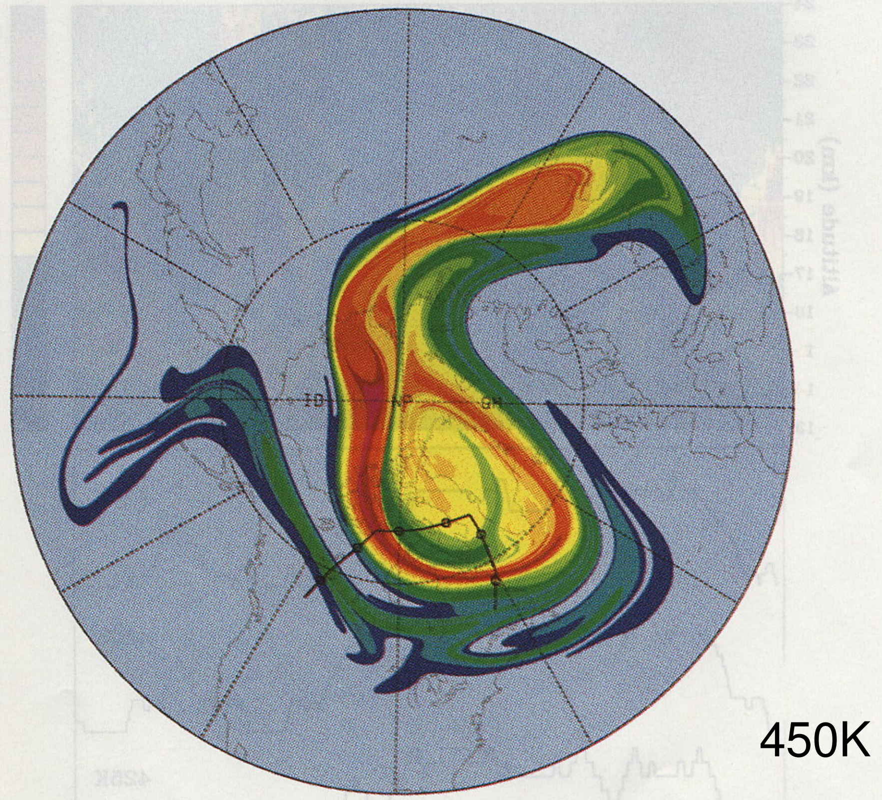

Plate 3. Vortex structure on the 450 K isentropic surface at 0000 UT on January 24, 1992, from the CAS integration of Plate 2. The DC-8 flight track for this day is shown. (The part of the flight track that is shown here is that for which data are plotted on Plate 4; circles correspond to the hours marked on Plate 4.)

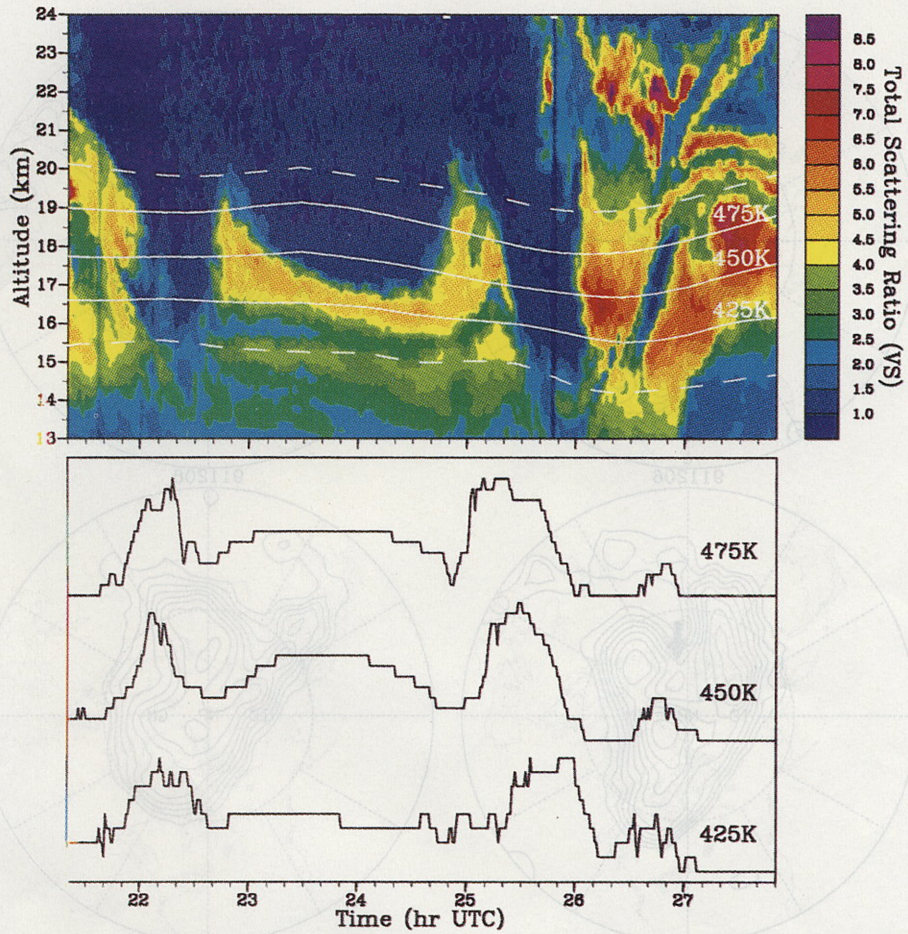

Plate 4. Cross sections of the vortex above the DC-8 flight track on January 23–24, 1992. (top) Aerosol scattering ratio measured from the DC-8 lidar as a function of time, with the altitudes of the 400 K (dashed curve, bottom), 425 K, 450 K, 475 K (solid curve), and 500 K (dashed curve, top) isentropes superimposed. (bottom) Vortex structure at 425, 450, and 475 K as determined from the CAS integrations at 0000 UT on January 24. Plotted for each material contour are the values of potential vorticity associated with each at the start of the calculation. Thus high values correspond to vortex air, and low values correspond to extravortex air.

intrusion

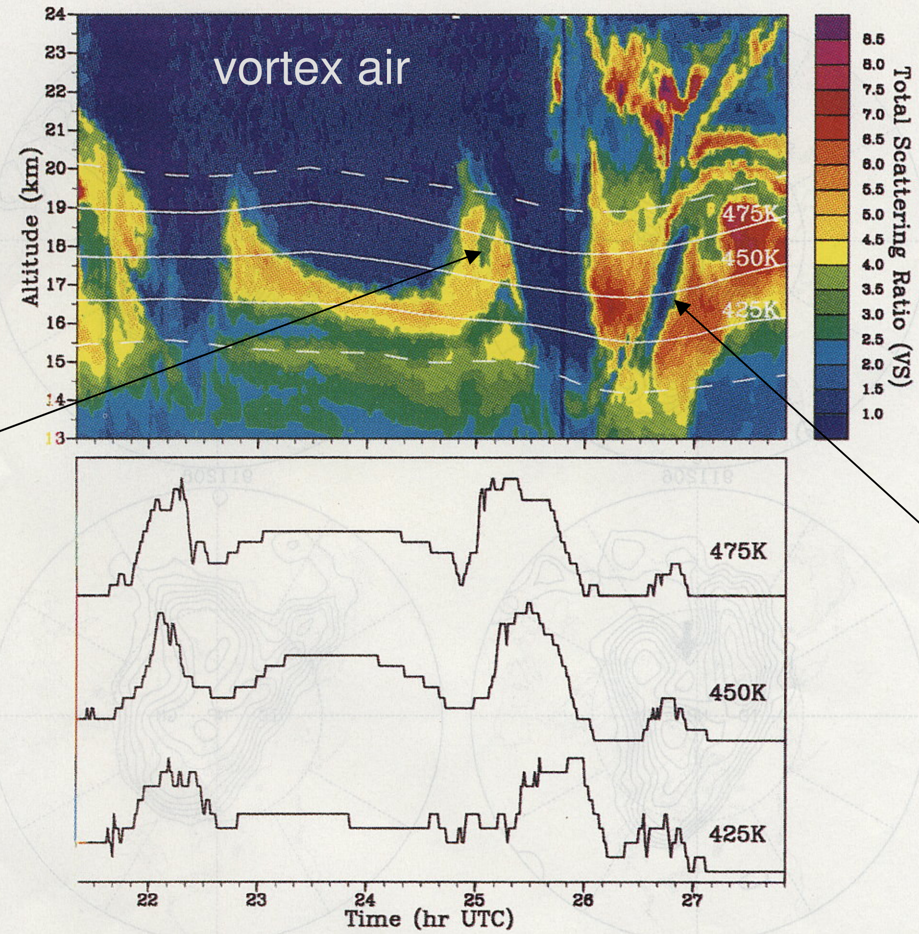

vortex filament

Plate 4. Cross sections of the vortex above the DC-8 flight track on January 23–24, 1992. (top) Aerosol scattering ratio measured from the DC-8 lidar as a function of time, with the altitudes of the 400 K (dashed curve, bottom), 425 K, 450 K, 475 K (solid curve), and 500 K (dashed curve, top) isentropes superimposed. (bottom) Vortex structure at 425, 450, and 475 K as determined from the CAS integrations at 0000 UT on January 24. Plotted for each material contour are the values of potential vorticity associated with each at the start of the calculation. Thus high values correspond to vortex air, and low values correspond to extravortex air.

(iii) Rossby waves and the stratospheric circulation

Driving the residual circulation

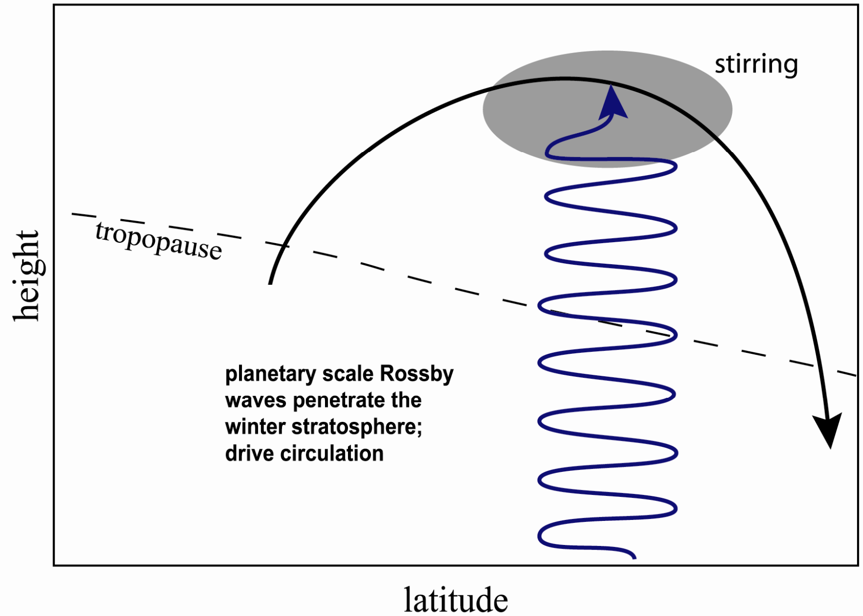

$$\cancel{\frac{\partial A}{\partial t}} + \nabla \cdot \mathbf{F} = \mathit{dissipation}$$

$$\cancel{\frac{\partial \bar{u}}{\partial t}} - 2\Omega \sin\varphi \bar{v}_* = \frac{1}{\rho}\nabla \cdot \mathbf{F} < \mathbf{0}$$

⟶ wave drag pumps flow poleward

$$\frac{1}{a\cos\varphi}\frac{\partial}{\partial\varphi}(\bar{v}_*\cos\varphi) + \frac{1}{\rho}\frac{\partial}{\partial z}(\rho\bar{w}_*) = 0$$

$$\rho\bar{w}_* = -\frac{1}{a\cos\varphi}\frac{\partial}{\partial\varphi}\cos\varphi\int_z^\infty \rho\bar{v}_*\, dz$$

⟶ “downward control” [Haynes et al, *J Atmos Sci*, 1981] explicit solutions

$$
\begin{aligned}
-2\Omega \sin\varphi \rho \bar{v}_* &= \nabla \cdot \mathbf{F} \\
\rho \bar{v}_* &= -\frac{\partial \chi_*}{\partial z} \\
\chi_* &= -\frac{1}{2\Omega \sin\varphi} \int_z^\infty \nabla \cdot \mathbf{F} \, dz
\end{aligned}
$$

→ wave drag must penetrate into tropics to explain tropical upwelling

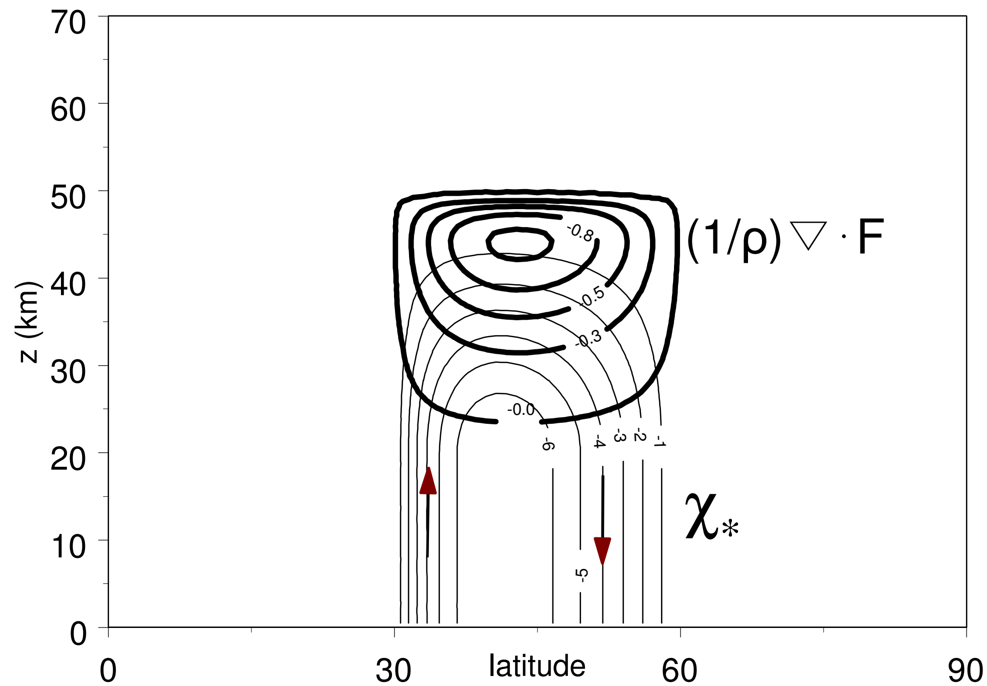

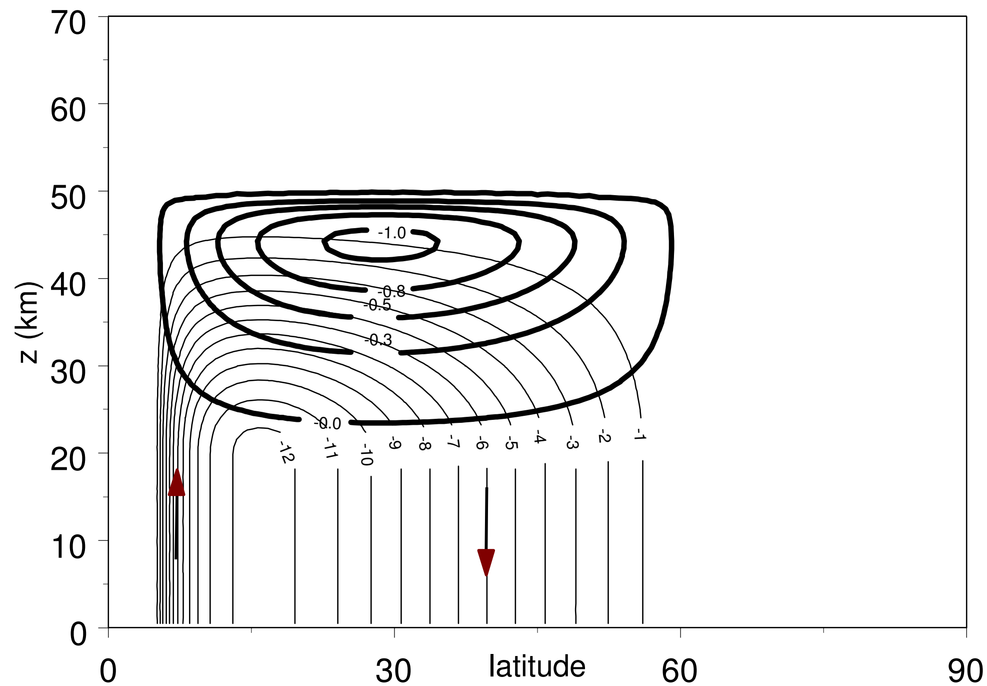

1992 September 6

southern hemisphere
middle stratosphere

10 hPa

geopotential
height (m)

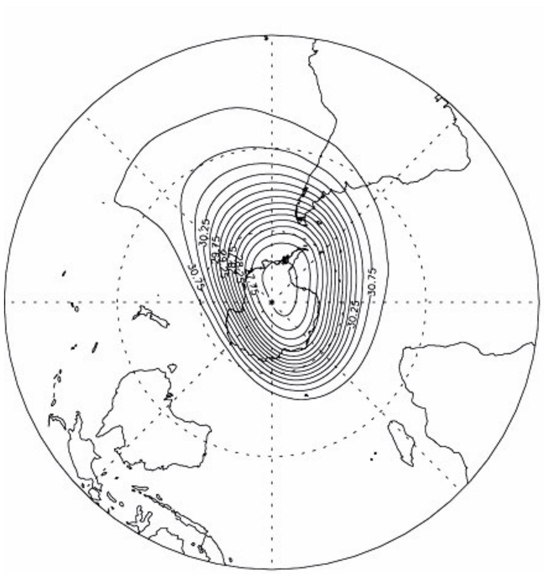

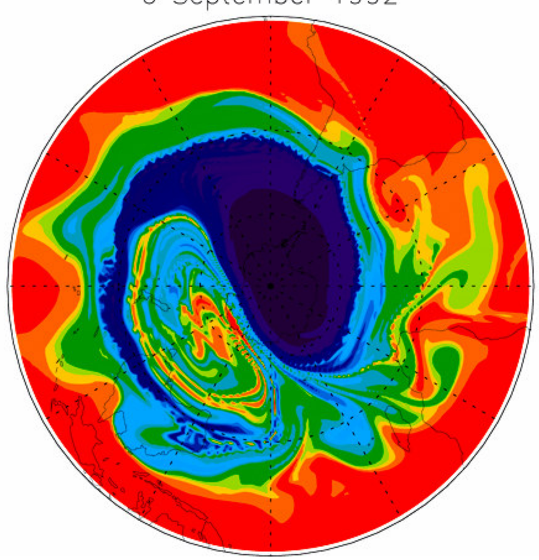

10 hPa

radiative heating
(K day^{-1})

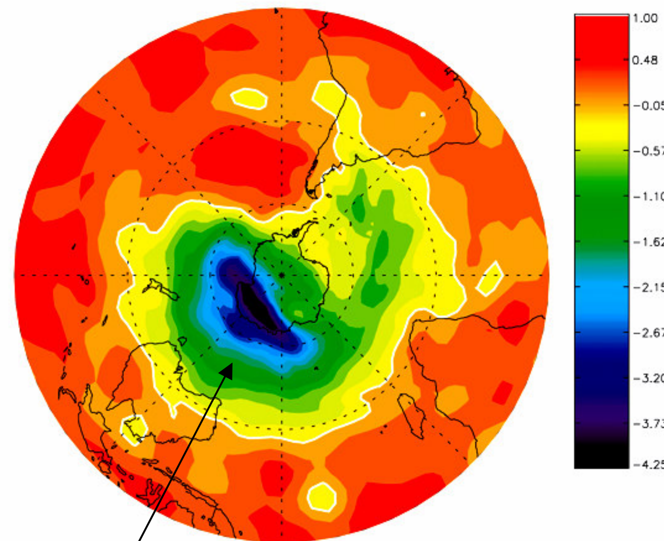

strongest downwelling / radiative
cooling at edge of vortex

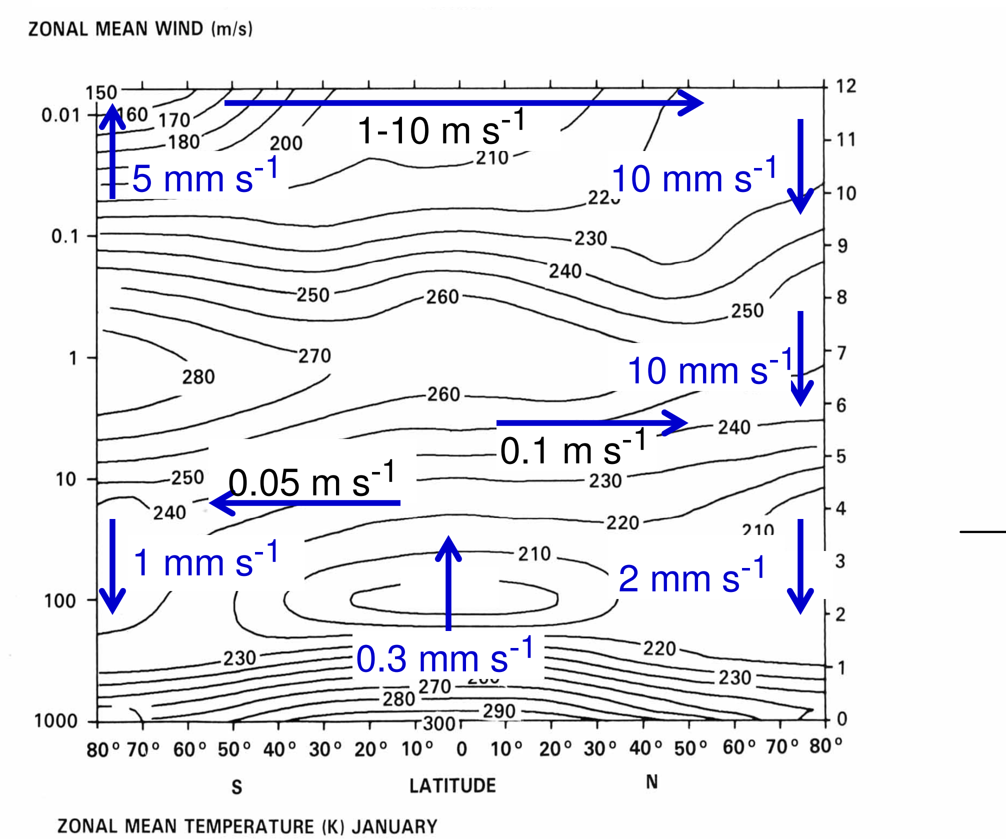

Rossby wave drag can account for circulation in stratosphere, but not mesosphere

→ need gravity wave drag in mesosphere

(iv) Gravity waves and the mesospheric circulation

Internal gravity waves

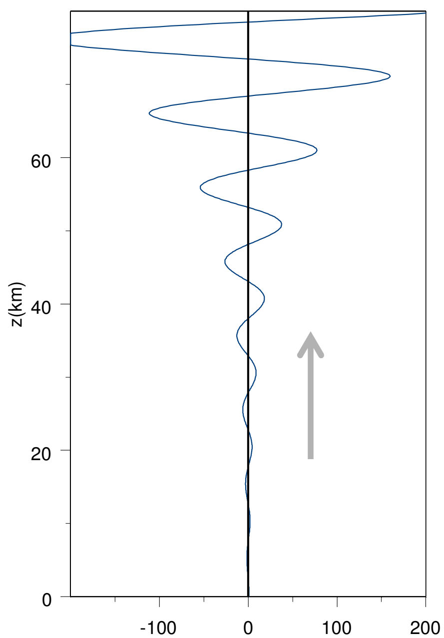

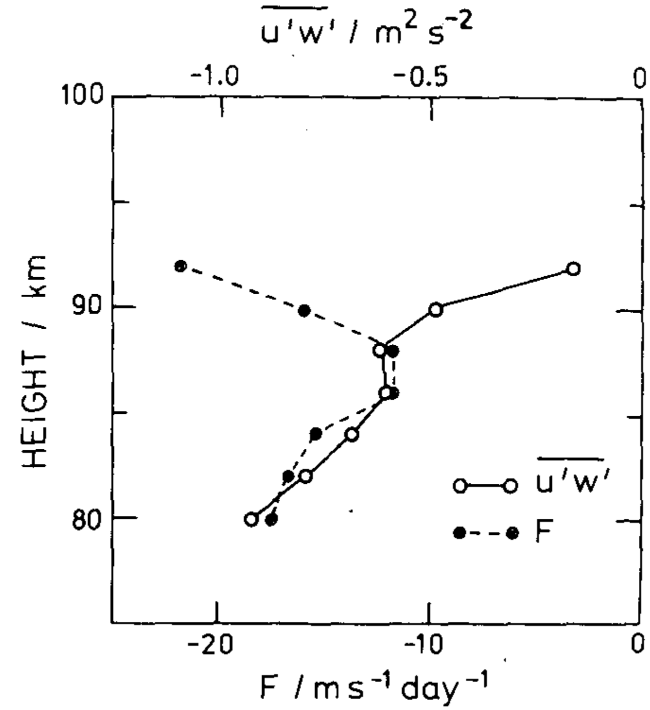

FIG. 6. Height profiles of the upward flux of zonal momentum ($\overline{u'w'}$) for the period 11–14 May 1981 (open circles) and the associated body force F (solid circles).

[Vincent & Reid, *J Atmos Sci*, 1983]

$$\overline{u'w'} \sim 1 \text{ m}^2\text{s}^{-2}$$

$$\rightarrow \frac{1}{\rho}\nabla \cdot \mathbf{F} \simeq \frac{1}{\rho}\frac{\partial}{\partial z}\left(\rho\overline{u'w'}\right)$$

$$\sim 1 \times 10^{-4}\text{ms}^{-2}$$

$$\sim 10 \text{ ms}^{-1}\text{day}^{-1}$$

$$\rightarrow \bar{v}_* \sim 1 \text{ ms}^{-1}$$

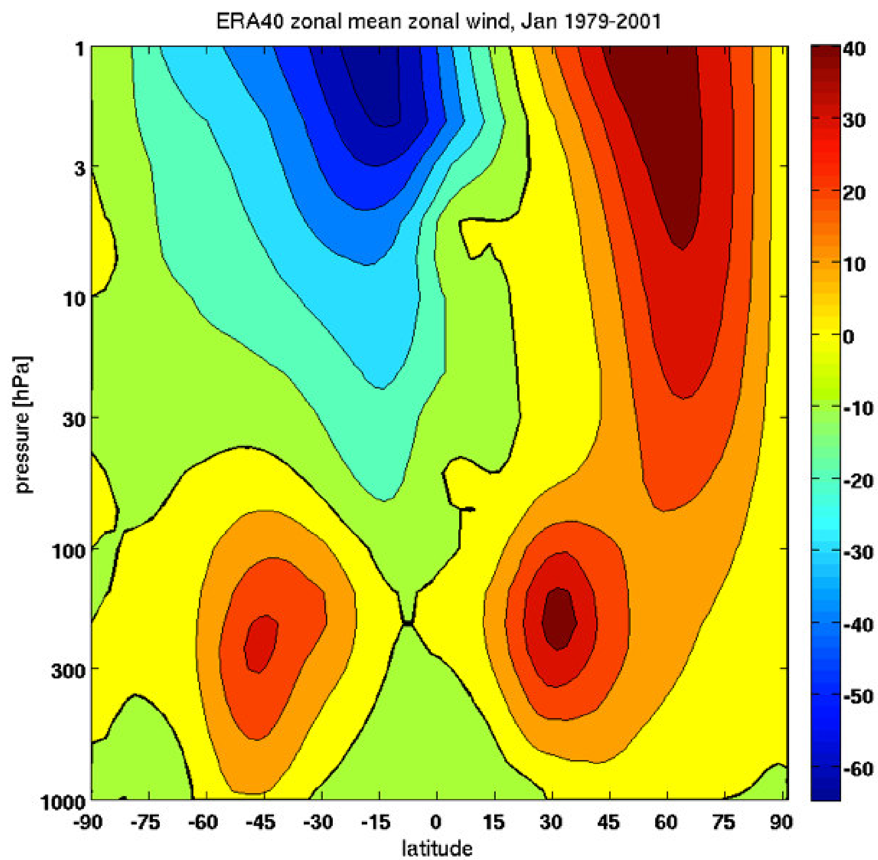
ERA40 zonal mean zonal wind, Jan 1979-2001
pressure [hPa]
latitude
1
3
10
30
100
300
1000
-90 -75 -60 -45 -30 -15 0 15 30 45 60 75 90
40
30
20
10
0
-10
-20
-30
-40
-50
-60

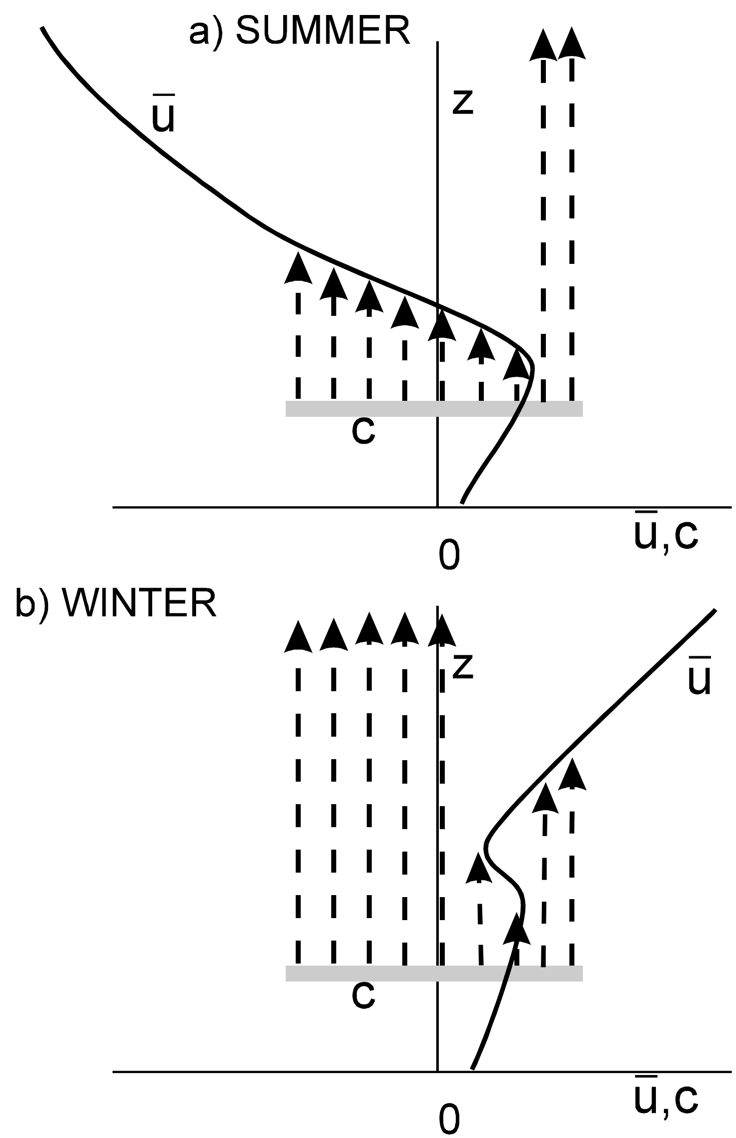
a) SUMMER
$\bar{u}$
z
c
0
$\bar{u}$,c
b) WINTER
z
$\bar{u}$
c
0
$\bar{u}$,c

solstice circulation

Westward gravity waves produce drag – pump flow poleward

Eastward gravity waves produce eastward force – pump flow *equatorward*

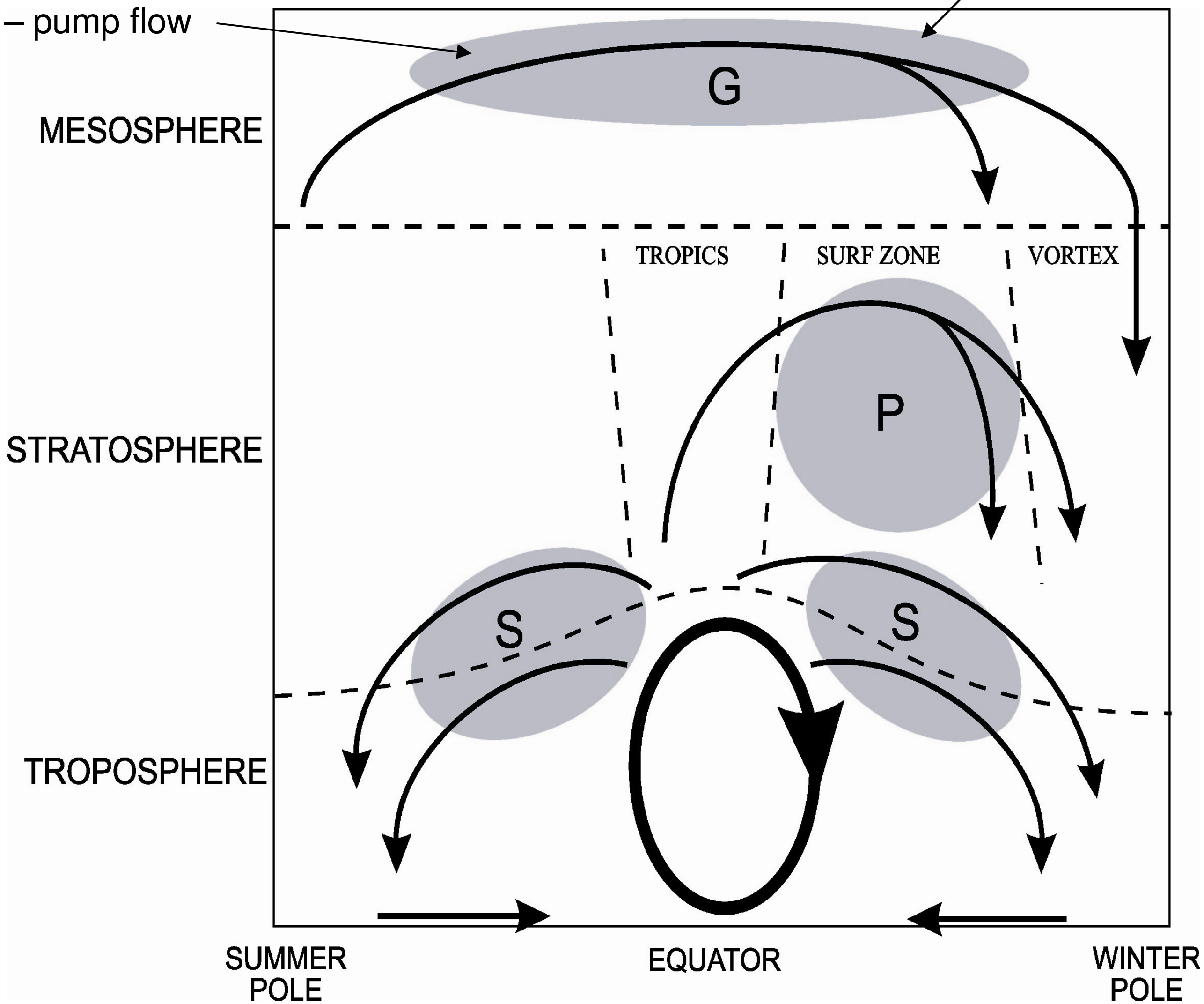

(v) Variability of the stratospheric circulation: wintertime vacillations and polar warmings

warm cold

Variability of North Pole temperatures

Monthly mean T, 30 hPa

- High degree of variability in winter
- (in spring in S Hem)
- i.e., during seasons of strong wave activity

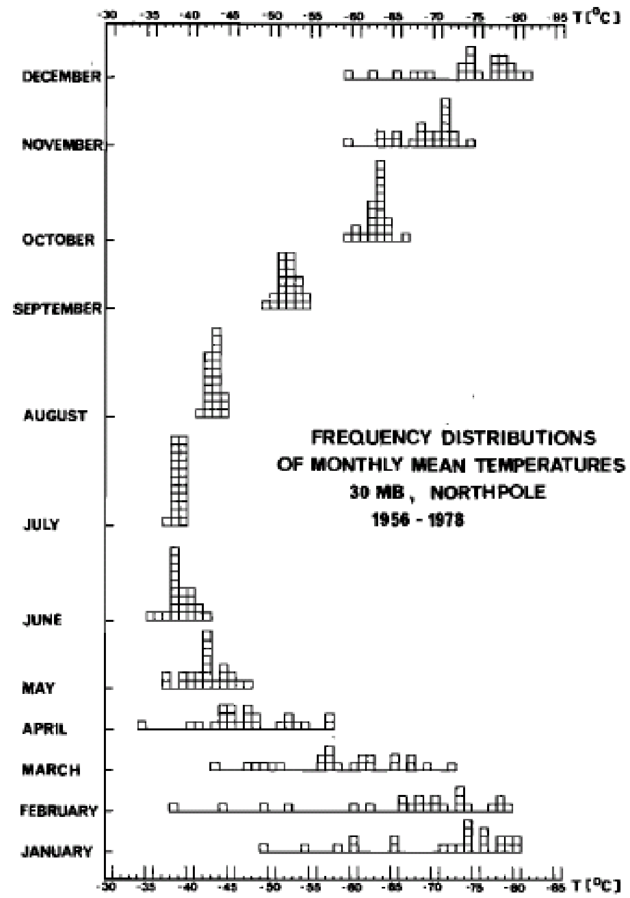

Fig. 17. Frequency distribution of monthly mean 30-mbar temperatures [°C] at the North Pole, 1956–1978 [from *Naujokat*, 1981*a*].

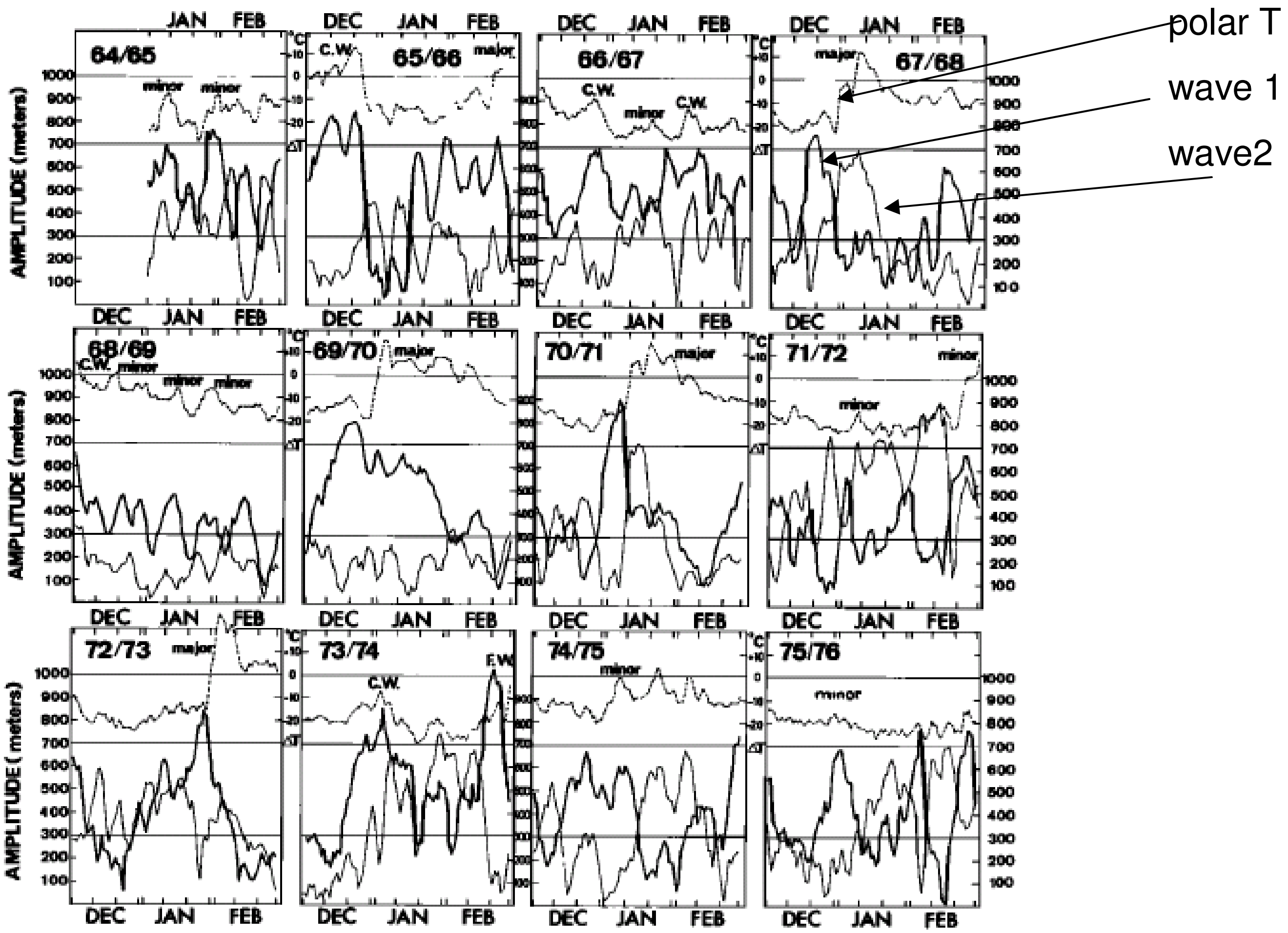

Fig. 10. Daily values of zonally averaged 30-mbar temperature differences [°C] between 80° and 50°N (ΔT, broken lines) and daily values of the amplitudes [geopotential m] of zonal harmonic height waves 1 (heavy lives) and 2 (thin lines) at 60°N, 30 mbar [from *Labitzke*, 1977*a*].

[Labitzke, *J Geophys Res,* 1981]

Major warming Jan 2009
10 hPa

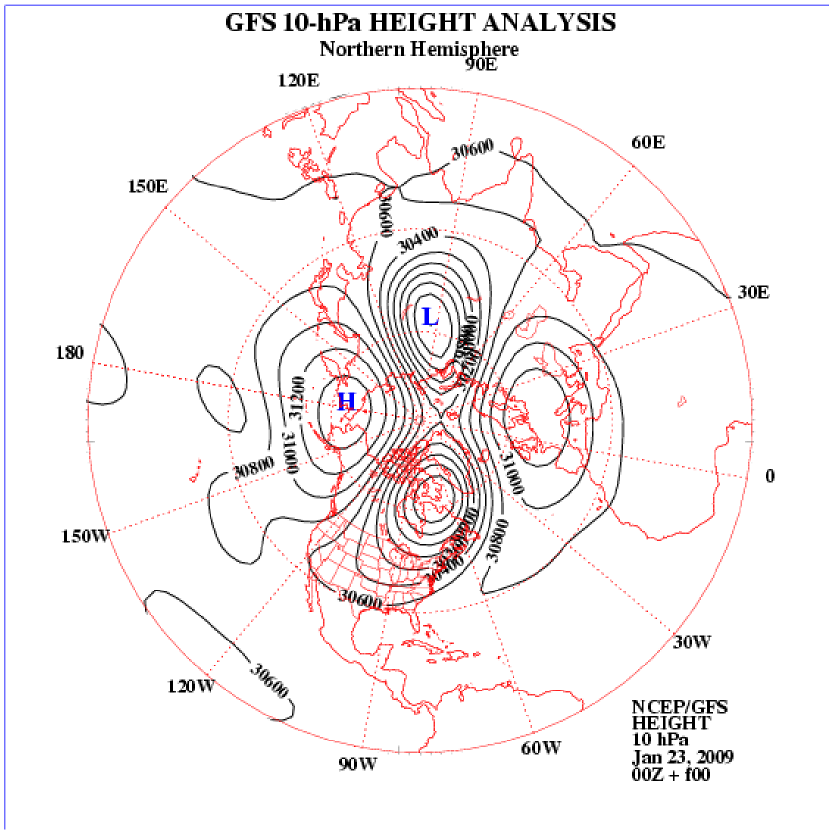

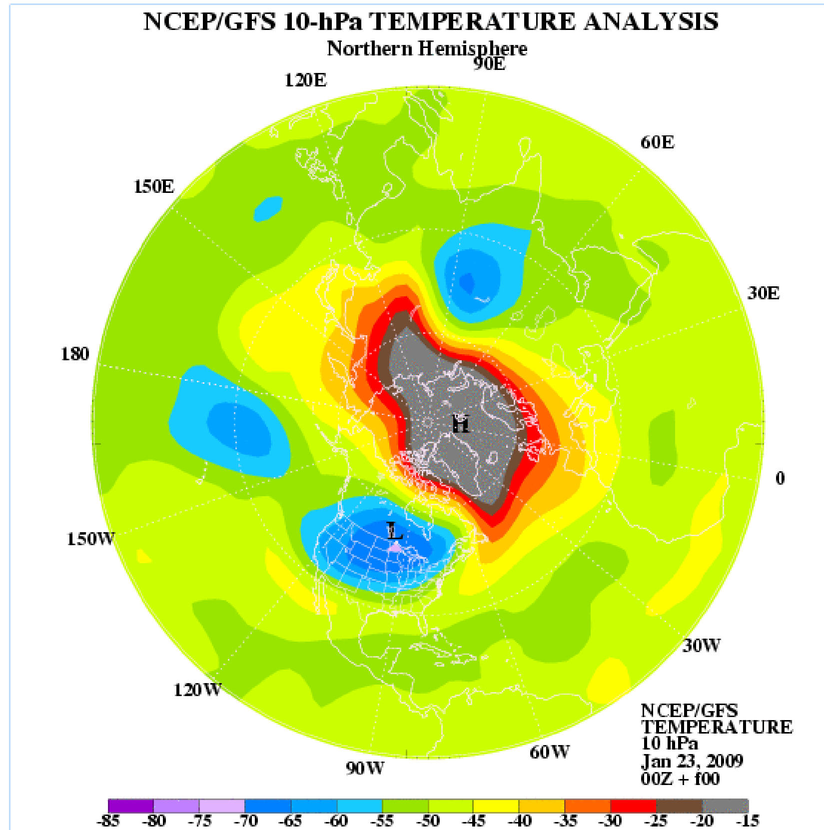

Polar warming as a response to wave amplification

[Matsuno, *J. Atmos. Sci.*, 1971]

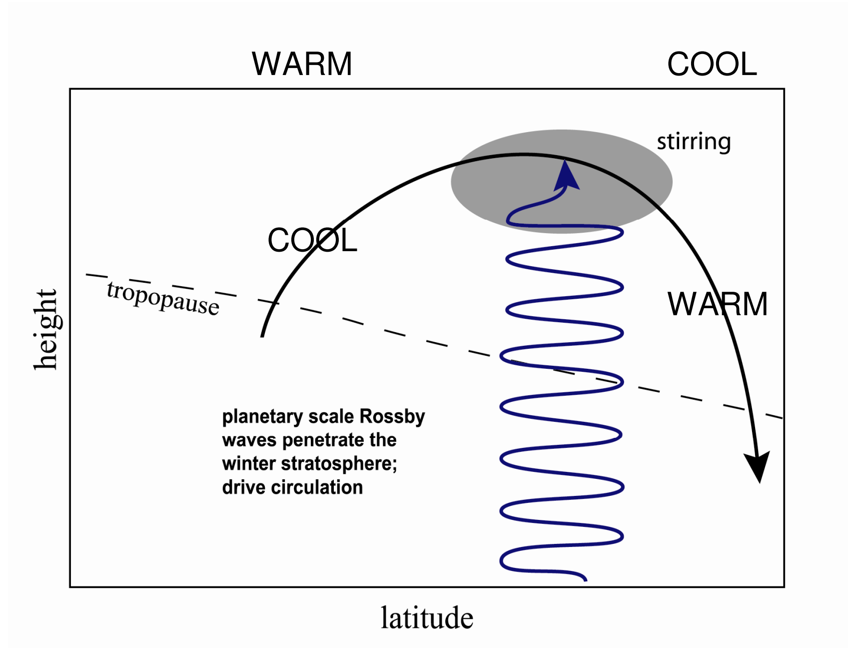

stage 1 (conservative):

$$\nabla \cdot \mathbf{F} = -\frac{\partial \mathbf{A}}{\partial t}$$

→ forms critical layer

stage 2 (no further growth, dissipative)

$$\nabla \cdot \mathbf{F} = \textit{dissipation}$$

Why do waves amplify?

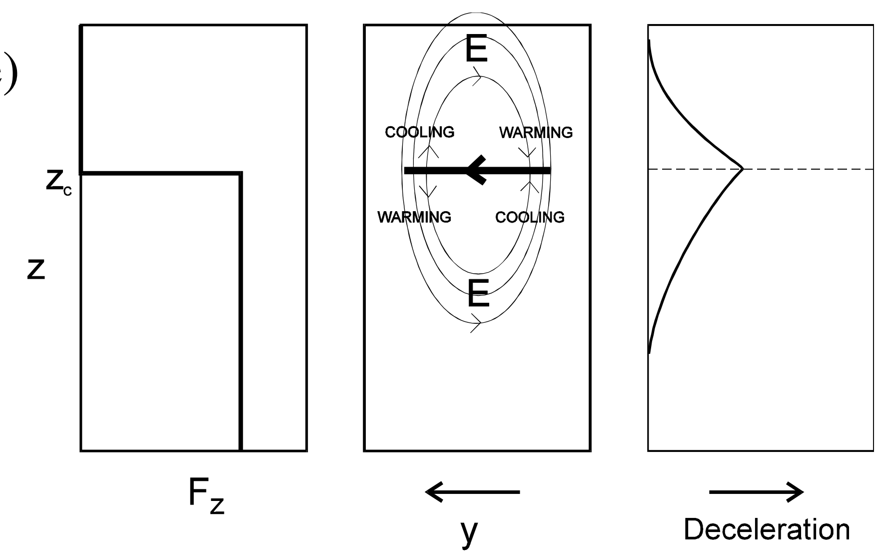

Vacillations in simple models

(Holton & Mass, *J. Atmos. Sci.* *, 1976)*

Truncated quasi-linear model

on midlatitude β – plane

$\bar{u} = U(z)\sin ly$

→ linear calculation for wave

→ $\nabla \cdot \mathbf{F} \rightarrow \partial\bar{u}/\partial t$

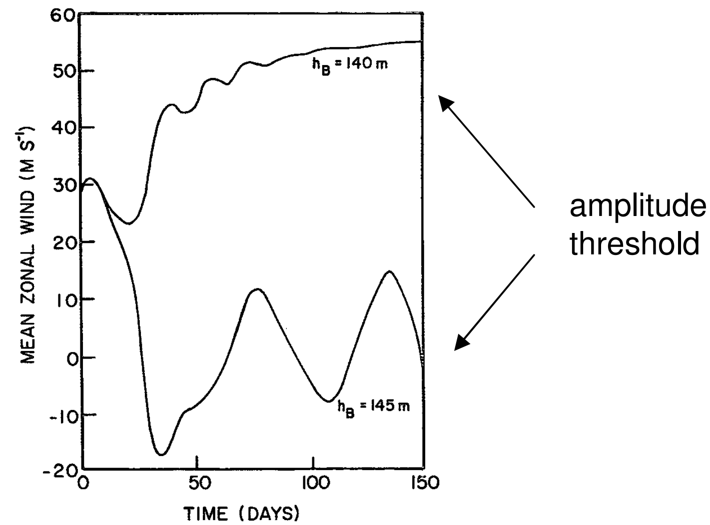

Fig. 2. Time evolutions of the mean zonal wind at 25 km and midchannel for the steady regime ($h_B = 140$ m)and the vacillating regime ($h_B = 145$ m) for zonal wavenumber 2 forcing.

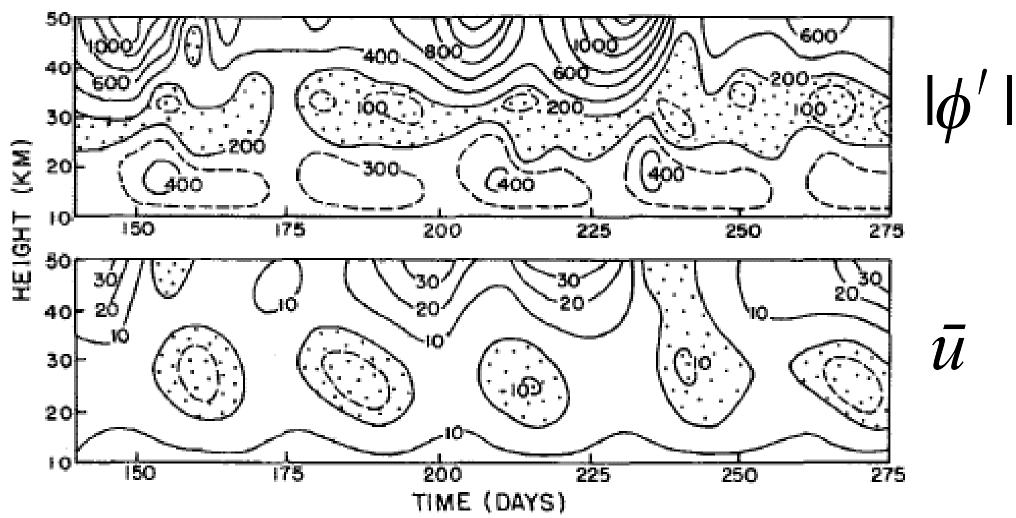

Fig. 6. Time-height sections of the geopotential height perturbation amplitude (upper) and the mean zonal wind (lower) for wavenumber 2 forcing with $h_B = 250$ m. Units: height (m), zonal wind (m s^{-1}). Stippling indicates regions of negative zonal wind and geopotential amplitudes less than 200 m.

Vacillations in GCMs [Scott & Polvani, *Geophys Res Lett*, 2004]

steady thermal forcing of Rossby wave

variability supressed in troposphere

→ vacillations stratospheric in origin

$\bar{u}(60^o N, z, t)$

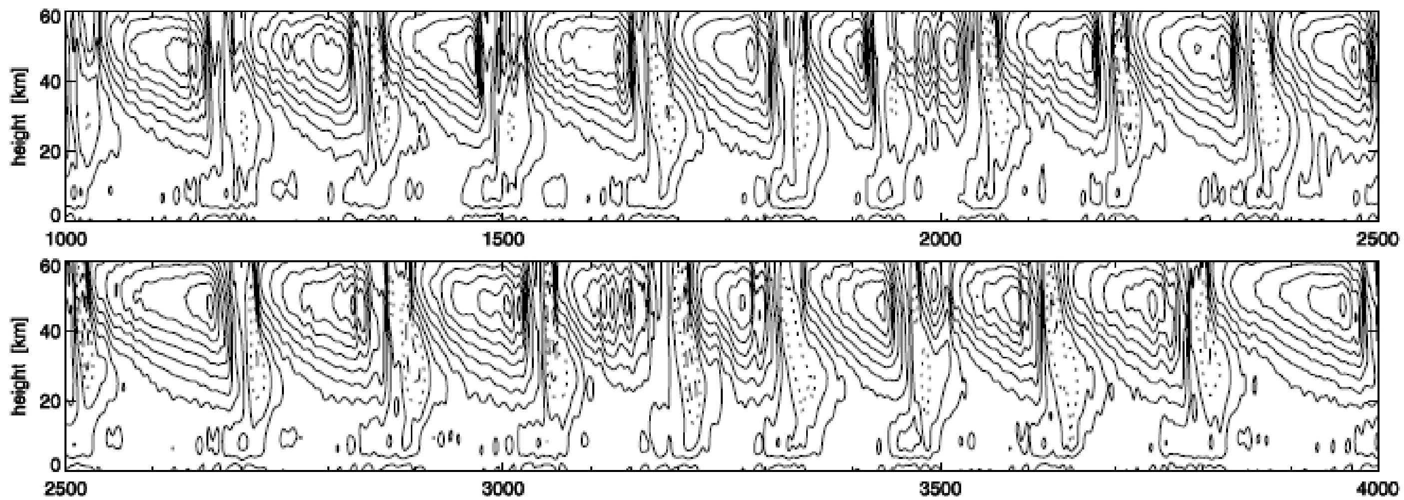

Figure 1. Zonal mean zonal velocity at 60°N as a function of height (in km) and time (in days). Numerical resolution is T42, with 40 vertical levels. The topospheric wave forcing amplitude $A = 2 \times 10^{-4}$ Ks^{-1}, and the radiative equilibrium vortex strength $\gamma = 2$. The contour interval is 10 ms^{-1}, with positive, negative, and zero values shown solid, dashed, and dotted, respectively.

Vacillations in GCMs [Scott & Polvani, *Geophys Res Lett*, 2004]

steady thermal forcing of Rossby wave

variability supressed in troposphere

→ vacillations stratospheric in origin

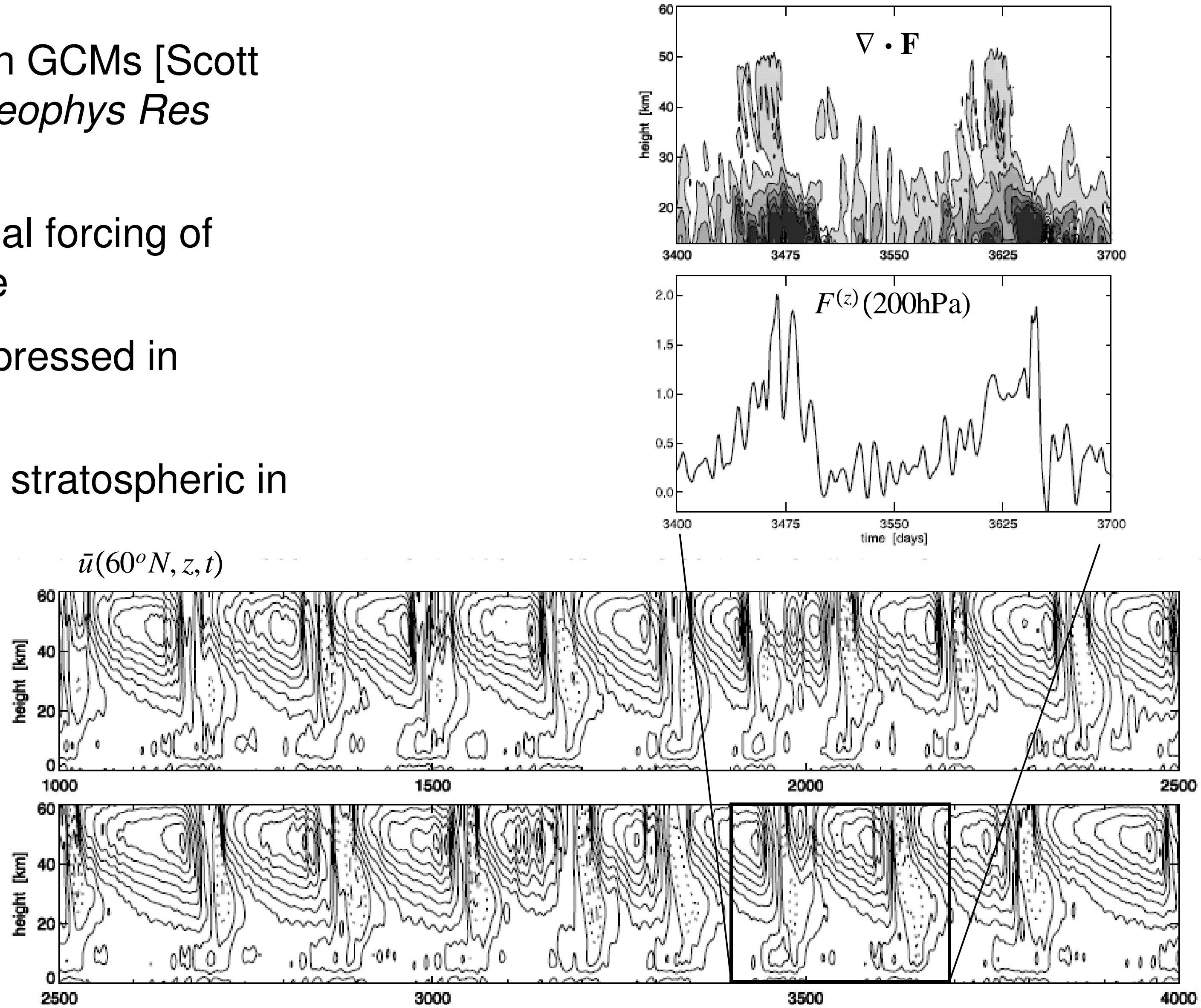

Figure 1. Zonal mean zonal velocity at 60°N as a function of height (in km) and time (in days). Numerical resolution is T42, with 40 vertical levels. The topospheric wave forcing amplitude $A = 2 \times 10^{-4}$ Ks^{-1}, and the radiative equilibrium vortex strength $\gamma = 2$. The contour interval is 10 ms^{-1}, with positive, negative, and zero values shown solid, dashed, and dotted, respectively.

(vi) Variability of the stratospheric circulation: the tropical quasi-biennial oscillation

Equatorial winds

(monthly mean anomalies)

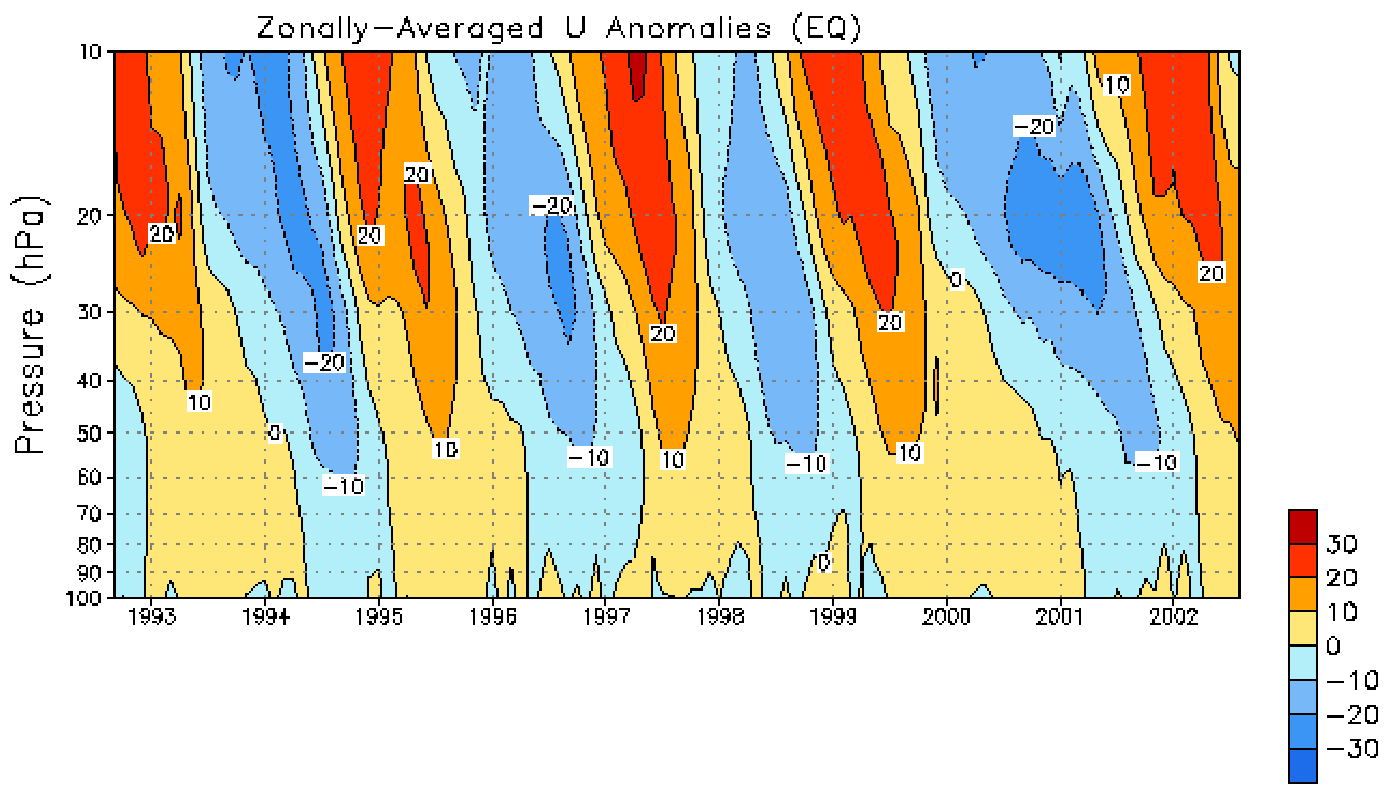

Irregular period around 27 months

Downward migration of westerlies and easterlies

Confined (mostly) within about 10 degrees of equator

Can be produced by 2 upward propagating waves of opposite zonal phase speed:

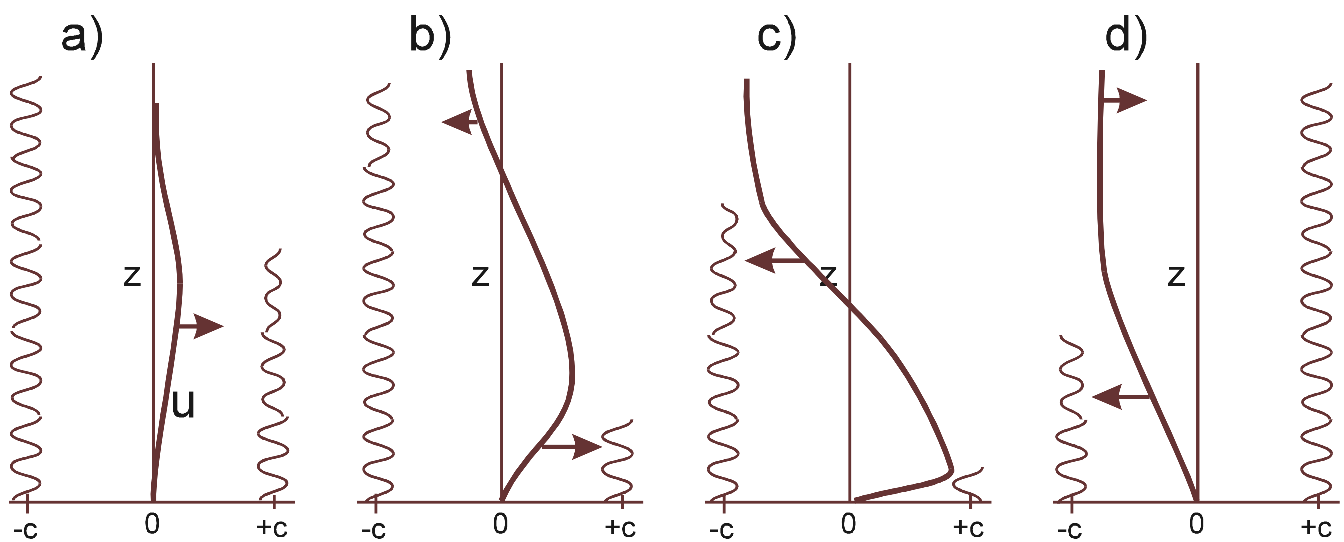

実験室の中の空と海

"QBO" in the lab

Atmosphere and Ocean in a Laboratory

subcritical forcing

実験室の中の空と海

Atmosphere and Ocean in a Laboratory

“QBO” in the lab

supercritical forcing

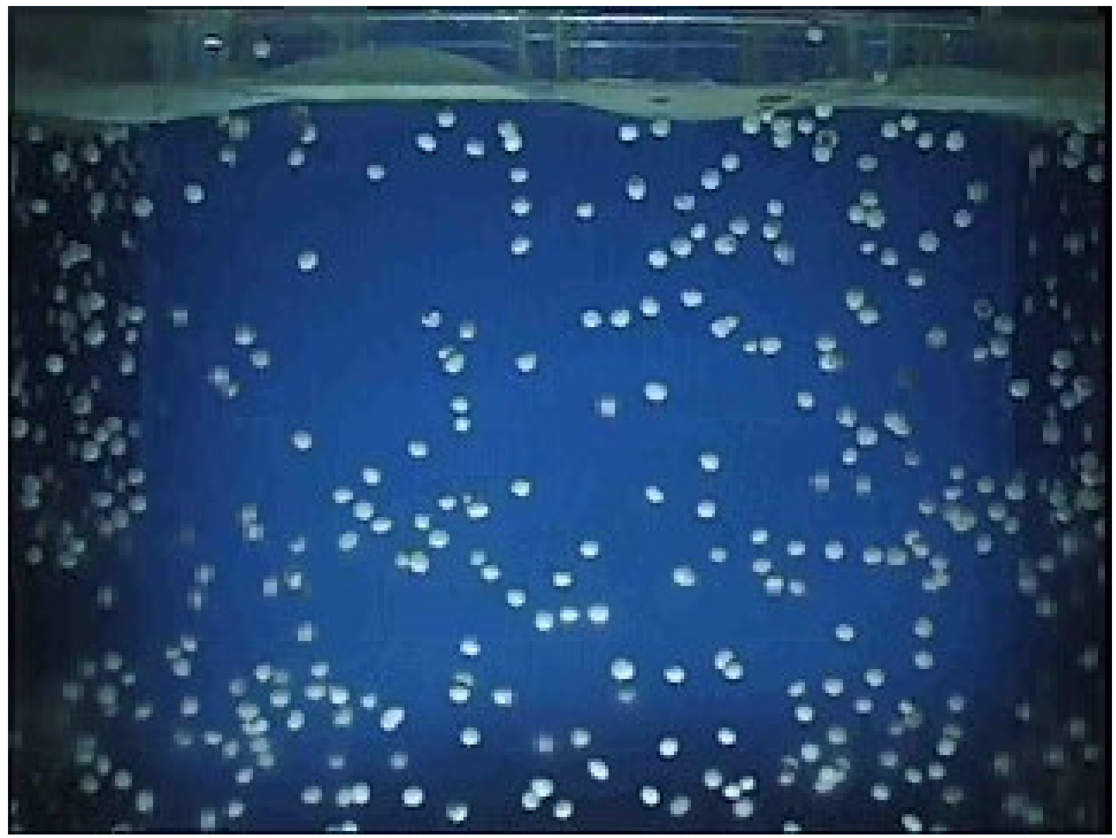

References

- Anderson, J. G., Brune W. H., Proffitt1989: Ozone Destruction by Chlorine Radicals Within the Antarctic Vortex: The Spatial and Temporal Evolution of ClO-O3 Anticorrelation Based on in Situ ER-2 Data, J. Geophys. Res., 94, 11465-11479
- K. Labitzke, 1981: Stratospheric-Mesospheric Midwinter Disturbances: A Summary of Observed Characteristics, J. Geophys. Res, 86, 9665-9678
- Mahlman, J. D., Umscheid, L. J., 1984: Dynamics of the middle atmosphere: Successes and problems of the GFDL "SKYHI" general circulation model, Terra Scientific Publishing Company, 501-525 pp.
- McIntyre, M. E., Palmer, T.N., 1983: Breaking planetary waves int the stratosphere, Nature, 305, 593-600
- Naujokat, B., 1981: Long-Term Variations in the Stratosphere of the Northern Hemisphere During the Last Two Sunspot Cycles, J. Geophys. Res., 86, 9811-9816

References

- Plumb, R. A., 2002: Stratospheric Transport, J. Met. Soc. Japan, 80, 793-809
- Plumb, R. A., 2007: Tracer interrelationships in the stratosphere, Rev. Geophys., Vol. 45, RG4005, 1-33
- Rosenlof, 1995: Seasonal cycle of the residual mean meridional circulation in the stratosphere, J. Geophys. Res., 100, 5173-5191
- Waugh, D. W., Plumb, R. A., Atkinson, R. J., Schoeberl, M. R., Lait, L. R., Newman, P. A., Loewenstein, M., Toohey, D. W., Avallone, L. M., Webster, C. R., May, R. D., 1994: Transport out of the lower stratospheric Arctic vortex by Rossby wave breaking, J. Geophys. Res., 99, 1089-1105
- NCEP, http://www.cpc.noaa.gov/
- Atmosphere and Ocean in a Laboratory, http://www.gfd-dennou.org/library/gfd_exp/index.htm